RESEARCH ARTICLE SUMMARY

IMMUNOLOGY

Macrophage MR1 antigen presentation promotes MAIT cell immunity and lung microbiota modulation

Jieru Deng† and Yuting Yan† *et al.*

Full article and list of author affiliations: https://doi.org/10.1126/science.adr6322

INTRODUCTION: The immune system consists of cells that detect microorganisms with varying degrees of selectivity. Many cell types react against components found in most viruses or bacteria, whereas only a few among a huge number of T and B lymphocytes react against a specific fragment of an individual pathogen. Mucosal associated invariant T cells (MAIT cells) sit between these extremes. They are abundant but highly specific for vitamin B–derived antigens (VitBAg), small molecules produced only by bacteria and fungi. VitBAg detection enables MAIT cells to "sense" and interact with the healthy microbiome and to respond against pathogens. However, MAIT cells can only detect VitBAg that have been captured and displayed, bound to the receptor MR1, on the surface of antigen-presenting cells (APCs). The identity of this APC has remained elusive, hampering development of therapies that might exploit the immune functions of MAIT cells.

RATIONALE: The MR1-MAIT cell axis is highly conserved in mammals. It was reasonable to assume that a specific cell type would also have a conserved, dominant role in MR1-VitBAg presentation. We hypothesized that such an APC would synthesize more MR1 protein, obtain microbial VitBAg more effectively, and display higher levels of MR1-VitBAg complexes than those of other cells. We generated a genetically modified mouse strain in which cells accumulate a fluorescent protein at levels proportional to the amount of MR1 they produced. This facilitated identification of candidate APCs specialized at VitBAg presentation in tissues that we could investigate to determine their ability to capture VitBAg, produce MR1-VitBAg complexes, and engage in interactions with MAIT cells. In addition, selective deletion of MR1 in candidate APCs would allow their relevance in regulating MAIT cell function to be understood.

RESULTS: In mice, MR1 expression was greatest in tissue-resident macrophages, particularly in lung and body cavity macrophages. Similarly in humans, macrophages had the greatest levels in lung and spleen cells examined. MR1 protein abundance was increased in macrophages through tissue-specific environmental cues and microbiota-derived signals. These pathways depended on MyD88 expression in macrophages, indicating that Toll-like receptor signaling promoted MR1 expression. Mice in which MR1 expression was selectively eliminated in macrophages and other myeloid cells had normal numbers of MAIT cells. However, these mice showed an altered lung microbiota, mounted defective MAIT cell responses against infecting bacteria, and showed impaired pathogen clearance. Side-by-side comparisons of multiple cell types—including dendritic cells, B cells, and T cells—confirmed the superior ability of macrophages to carry out MR1-VitBAg presentation and MAIT cell activation.

CONCLUSION: Macrophages acted as MR1 APCs that orchestrated MAIT cell responses to microbial antigens. Their high MR1 expression, efficient ligand uptake, and tissue localization positions them as key regulators of MAIT cell–mediated immunity and microbiota homeostasis. Although other APCs may also present MR1-bound antigens, the extent of their involvement remains unclear. We propose that macrophages act as central players in MR1 antigen presentation and are potential targets for immunotherapeutic strategies that involve MAIT cells and MR1-restricted T cells. □

Corresponding authors: Jose A. Villadangos (j.villadangos@unimelb.edu.au); Hamish E. G. McWilliam (hamish.mcwilliam@unimelb.edu.au) †These authors contributed equally to this work.
Cite this article as J. Deng *et al.*, *Science* **391**, eadr6322 (2026); DOI: 10.1126/science.adr6322

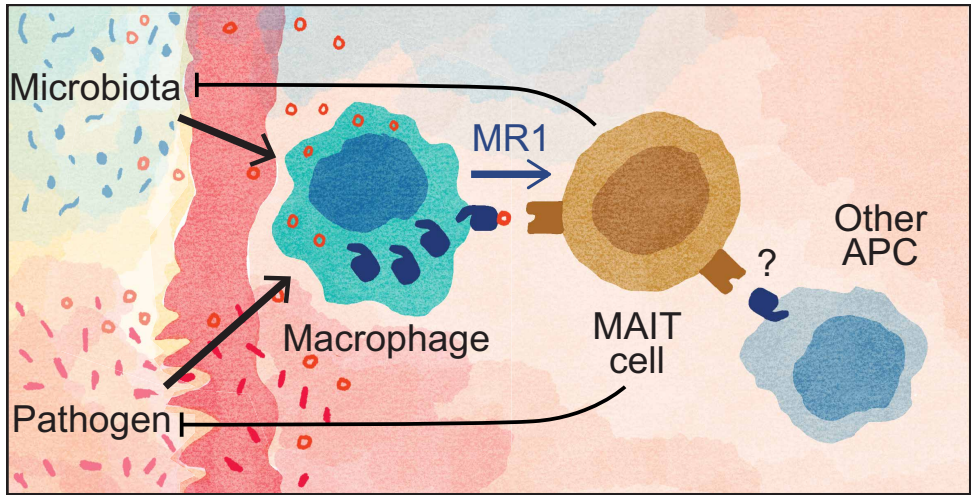

Macrophages are key MR1 APCs to MAIT cells. Macrophages express high levels of MR1 and are primed to capture vitamin B–related antigens that originate from the microbiota or bacterial pathogens. These antigens are presented to MAIT cells, triggering their activation. Once activated, MAIT cells can modulate the composition of the microbiota or help to control pathogenic infections.

IMMUNOLOGY

Macrophage MR1 antigen presentation promotes MAIT cell immunity and lung microbiota modulation

Jieru Deng[1]†, Yuting Yan[1,2,3]†, Xiaoyue Zhang[1], Calum J. Walsh[1,4], Emmanuel Montassier[5,6], Debajyoti Sinha[5,6], Huimeng Wang[1], Atieh Mousavizadeh[1], Mitra Ashayeripanah[1], Jeffrey Y. W. Mak[7], Hui-Fern Koay[1], Tobias Poch[1], Yannick O. Alexandre[1], Scott N. Mueller[1], Ajithkumar Vasanthakumar[8,9], Tim P. Stinear[1,4], Vanta J. Jameson[1,10], Alexis Perez-Gonzalez[1,10], Jenny Kingham[11], Tri Giang Phan[11,12], Nikita Potemkin[1,13], Lachlan Dryburgh[1,13], Jan Schroeder[1,13], David P. Fairlie[7], Laura K. Mackay[1], Zhenjun Chen[1], Laura Cook[1,14,15], Abderrahman Hachani[1,4], Alexandra J. Corbett[1], Antoine Roquilly[1,5,6], Jose A. Villadangos[1,16]*, Hamish E. G. McWilliam[1]*‡

Mucosal-associated invariant T cells (MAIT cells) mediate tissue homeostasis and antimicrobial immunity. However, the cells that express major histocompatibility complex (MHC) class I–related protein 1 (MR1) and present microbial vitamin B–derived antigens (VitBAg) to MAIT cells remain unknown. We found that MR1 expression varied across tissues and cell types. Macrophages from the lung and peritoneal cavity expressed the highest levels of MR1 and were the most efficient at capturing and presenting VitBAg to MAIT cells. Expression of MR1 in macrophages was regulated transcriptionally and induced by the tissue environment and microbiota. Depletion of MR1 in macrophages, dendritic cells, and monocytes changed the composition of the microbiota and impaired MAIT cell responses against bacterial infection. We concluded that macrophages are key for MR1 antigen presentation and MAIT cell immunity.

Major histocompatibility complex (MHC) class I–related protein 1 (MR1) displays antigens (Ag) on the cell surface for recognition by mucosal-associated invariant T cells (MAIT cells) (*1*–*3*). The Ag presented by MR1 are modified metabolites that are a by-product of microbial biosynthesis of riboflavin (vitamin B2) (*2*, *3*); hence, they are called vitamin B–related Ag (VitBAg). Because riboflavin is synthesized by most bacteria and fungi but not mammals (*3*, *4*), detection of VitBAg bound to MR1 alerts the immune system to the presence of microbes, whether they are normal components of the microbiota or infectious agents.

The structure of MR1 and of the T cell receptors (TCRs) used by MAIT cells to recognize MR1-VitBAg complexes (*5*) are highly conserved in mammals. Such coevolution implies a strong selective pressure to maintain this microbe-detection mechanism (*6*). MAIT cells are abundant in barrier tissues, where upon recognition of MR1-VitBAg complexes they secrete inflammatory cytokines (*7*), kill cells (*8*), and elicit tissue repair (*9*, *10*). Such activities enable MAIT cells to participate in tissue and microbiota homeostasis (*11*) and protective immunity against bacteria (*8*, *12*–*18*) and viruses (*19*). In addition, MAIT cells contribute to autoimmune and inflammatory reactions (*20*, *21*). Consequently, MAIT cells are attractive targets for the development of immunotherapeutic strategies to treat disease.

The antigen presenting cells (APCs) that display MR1-VitBAg complexes to MAIT cells remain uncharacterized (*13*, *14*, *16*, *17*, *22*). MR1 transcription can be detected in most cell types (*23*, *24*) but at such low levels that it is difficult to ascertain the functional relevance. Furthermore, MR1 expression is tightly controlled posttranslationally (*25*). In the absence of VitBAg, the small amount of MR1 protein produced by cells is retained in the endoplasmic reticulum (ER) (*24*), hampering identification of MR1-expressing cells. VitBAg can reach the lumen of the ER, where they bind covalently to MR1 through formation of a Schiff base bond (*5*). This triggers transport of the MR1-VitBAg complexes to the plasma membrane of the MR1 APC (*24*), where the complexes are recognized by the MAIT TCR. The identification of the APC remains challenging because the number of MR1-VitBAg complexes required for MAIT cell recognition is below the limit of detection of commonly used antibody-based methods. The identity of the MR1 APC is therefore unknown. This gap in knowledge hampers the development of strategies to harness the MR1-MAIT cell axis for prophylactic or therapeutic outcomes (*25*).

We generated a mouse strain with a fluorescent reporter that allowed us to compare MR1 expression in various hematopoietic and nonhematopoietic cell types in multiple tissues. This allowed us to identify the cells that express the highest levels of MR1 and to test their roles in microbiota homeostasis and MAIT cell responses against bacterial infection.

Results

A *Mr1*-reporter mouse model reveals transcription and protein expression

We generated a mouse strain in which the *Mr1* gene was replaced with the coding sequence for tdTomato fluorescent protein (TOM) (Fig. 1A). Homozygous reporter mice ($Mr1^{TOM}$) lacked MR1 expression and MAIT cells (*26*), whereas heterozygous animals ($Mr1^{TOM/WT}$) showed a slight but nonsignificant reduction in MAIT cell numbers (fig. S1A). To investigate whether TOM fluorescence was a valid surrogate of wild-type (WT) MR1 expression in these mice, we examined lung alveolar macrophages (AMΦ), which transcribe *Mr1* at higher levels than other cells (*27*). TOM was expressed at high levels in AMΦ; at very low levels in a small number of αβ T cells; and not at all in neutrophils, monocytes, or B cells (Fig. 1B). This expression pattern correlated well with the level of *Mr1* mRNA in lung cells of $Mr1^{WT}$ mice (Fig. 1C).

MR1 is retained in the ER and barely expressed on the cell surface in the steady state, but intracellular staining revealed AMΦ as the only lung cells that contained detectable levels of MR1 in WT mice (Fig. 1D, i, and fig. S1D, i). Upon binding VitBAg in the ER, MR1 translocates to the cell surface (*5*). We incubated WT cells with JYM87, a synthetic derivative of one of the canonical VitBAg called (2-oxopropylideneamino)-6-D-ribitylaminouracil (5-OP-RU). JYM87 recapitulates the main features of VitBAg but is more stable in solution (*28*, *29*). AMΦ were the only cells that displayed surface MR1 after this treatment (Fig. 1D, ii, and

[1]Department of Microbiology and Immunology, The Peter Doherty Institute for Infection and Immunity, The University of Melbourne, Melbourne, VIC, Australia. [2]School of Medicine, Tsinghua Medicine, Tsinghua University, Beijing, China. [3]Cancer Center, West China Hospital, Sichuan University, Chengdu, Sichuan, China. [4]Centre for Pathogen Genomics, at The Peter Doherty Institute for Infection and Immunity, The University of Melbourne, Melbourne, VIC, Australia. [5]Nantes Université, CHU Nantes, INSERM, Center for Research in Transplantation and Translational Immunology, UMR 1064, Nantes, France. [6]CHU Nantes, INSERM, Nantes Université, Anesthesie Reanimation, Nantes, France. [7]Centre for Chemistry and Drug Discovery and ARC Centre of Excellence for Innovations in Peptide and Protein Science, Institute for Molecular Bioscience, The University of Queensland, Brisbane, QLD, Australia. [8]Olivia Newton-John Cancer Research Institute, Heidelberg, VIC, Australia. [9]La Trobe University, Bundoora, VIC, Australia. [10]Melbourne Cytometry Platform, The University of Melbourne, Parkville, VIC, Australia. [11]Garvan Institute of Medical Research, Darlinghurst, NSW, Australia. [12]St. Vincent's Healthcare Clinical Campus, School of Clinical Medicine, Faculty of Medicine and Health, UNSW Sydney, Darlinghurst, NSW, Australia. [13]Computational Sciences Initiative (CSI), The Peter Doherty Institute for Infection and Immunity, The University of Melbourne, Melbourne, VIC, Australia. [14]Department of Critical Care, Melbourne Medical School, The University of Melbourne, Parkville, VIC, Australia. [15]Division of Infectious Diseases, University of British Columbia, Vancouver, BC, Canada. [16]Department of Biochemistry and Pharmacology, Bio21 Molecular Science and Biotechnology Institute, The University of Melbourne, Parkville, VIC, Australia. ***Corresponding author. Email: hamish.mcwilliam@unimelb.edu.au (H.E.G.M.); j.villadangos@unimelb.edu.au (J.A.V.)** †These authors contributed equally to this work. ‡Present address: Proxima Bio, Melbourne, VIC, Australia.

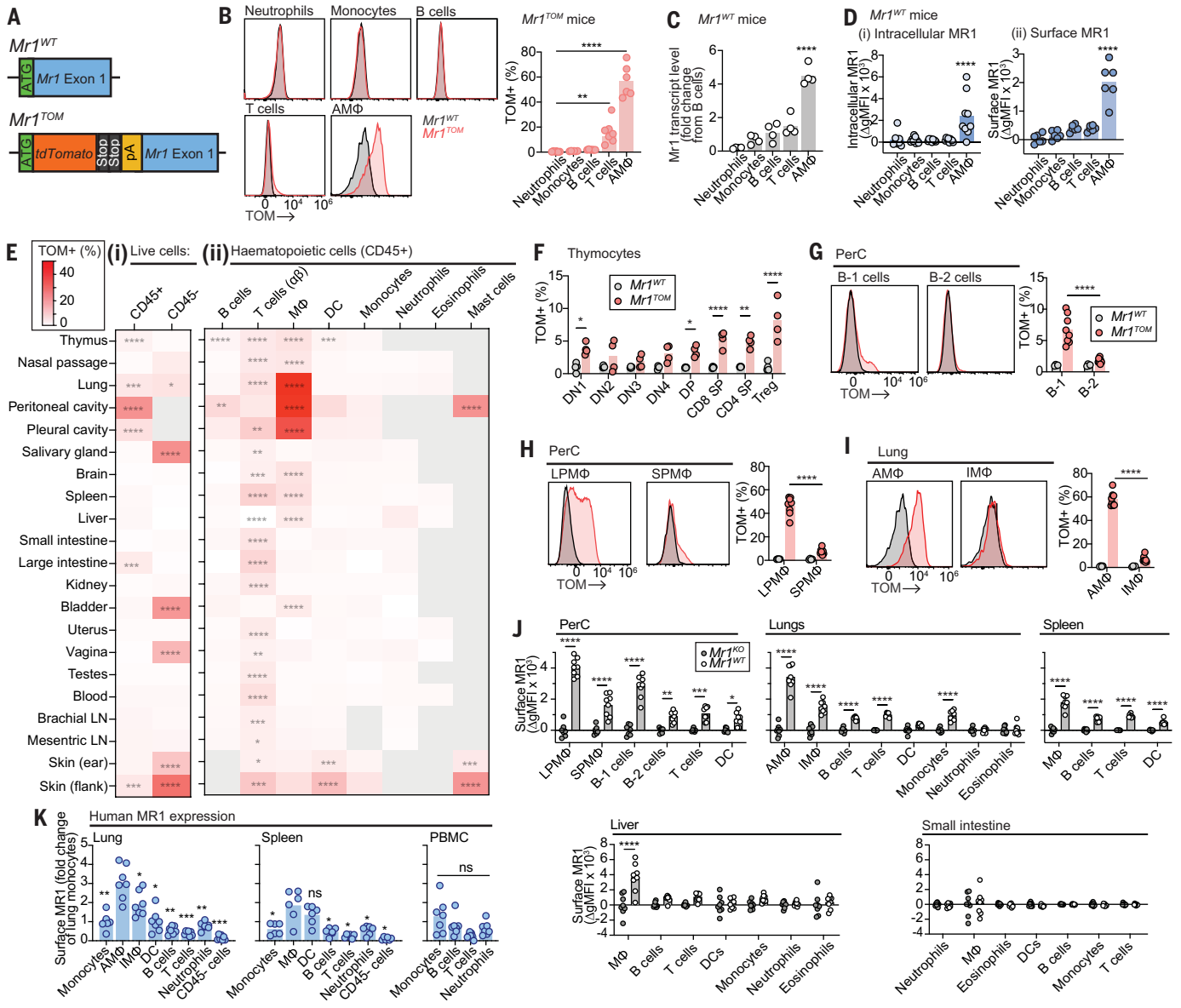

Fig. 1. The MR1-reporter mouse reveals cell- and tissue-specific MR1 expression. (**A**) Schematic diagram of the modification to the WT *Mr1* gene ($Mr1^{WT}$) for the MR1-tdTomato ($Mr1^{TOM}$) reporter mouse, in which the coding sequence for *tdTomato* (*TOM*) was inserted after the start codon (ATG) at exon 1, followed by two stop codons and a polyadenylate [poly(A)] signal. (**B**) The TOM expression in the indicated lung cell populations measured with flow cytometry from $Mr1^{WT}$ or $Mr1^{TOM}$ reporter mice. The signal is expressed as the percentage of TOM^+ cells of the whole population above $Mr1^{WT}$ background. (**C**) *Mr1* transcription levels in the indicated lung cell populations from $Mr1^{WT}$ mice represented as fold change of the B cell mean measured with qPCR. (**D**) (i) Intracellular content of MR1 detected with intracellular staining directly ex vivo without MR1 ligand or (ii) up-regulated MR1 protein level of the indicated lung cell populations from $Mr1^{WT}$ mice after 3 hours in vitro culture with the MR1 ligand JYM87 (10 μM). The MR1 level was adjusted for the background signal by subtracting the geometric mean fluorescence intensity (gMFI) of the $Mr1^{KO}$ from the $Mr1^{WT}$ samples (ΔgMFI). (**E**) Heat map of TOM^+ cells (%) from various organs of $Mr1^{TOM}$ mice of (i) total hematopoietic ($CD45^+$) or nonhematopoietic cells ($CD45^-$) or (ii) the indicated $CD45^+$ populations. Asterisks indicate whether TOM was significantly detected above background $Mr1^{WT}$ levels, and gray boxes indicate that the corresponding cell populations were not found. (**F**) TOM expression among thymocyte subsets. (**G**) TOM expression among B-1 and B-2 cells of the PerC. (**H**) TOM expression among MΦ subsets of the PerC (LPMΦ or SPMΦ). (**I**) TOM expression among MΦ subsets of the lung (AMΦ or IMΦ). (**J**) Up-regulated MR1 protein level (ΔgMFI) of the indicated cell populations from the PerC, lung, spleen, liver, or small intestine of $Mr1^{WT}$ mice after 3 hours in vitro culture with the MR1 ligand JYM87 (10 μM). (**K**) Up-regulated MR1 protein level (ΔgMFI adjusted for the blocked anti-MR1 stain) in the indicated cell populations from human donors after 3 hours in vitro culture with the MR1 ligand JYM87 (10 μM). Data are represented as fold change of monocytes. Bars and heat map data indicate the mean from at least two independent experiments in (B) to (K). Dots indicate individual mice [(B) $n = 6$; (C), $n = 4$; (D), $n = 6$ to 9; (E), $n = 5$ to 8; (F), $n = 4$; (G) to (J), $n = 8$ to 10] or individual human donors [(K), $n = 6$ or 7], and representative flow cytometry histograms are shown [(B) and (G) to (I)]. Gating strategies for the main mouse organs (fig. S2) and human tissues (fig. S5A) were provided in supplementary figures. Statistical significance was calculated by using [(B) to (D) and (K)] one-way or [(E) to (J)] two-way ANOVA followed by a multiple comparison test in which $*P < 0.05$, $**P < 0.01$, $***P < 0.001$, $****P < 0.0001$, or not significant (n.s.).

fig. S1D, ii). We concluded that the level of TOM fluorescence in cells of *Mr1*^{TOM} mice correlated with *Mr1* transcription and protein expression by their WT counterparts.

The tissue- and cell type–restricted expression of MR1 in mice and humans

Using TOM fluorescence as a surrogate of MR1 expression allowed us to generate an atlas of MR1 expression in complex single-cell suspensions of 21 organs and/or tissues of mice (Fig. 1E and fig. S2). TOM expression was detected in either the hematopoietic (CD45$^+$) or nonhematopoietic (CD45$^-$) compartments, but not both, in most tissues except the lungs and flank skin (Fig. 1E, i).

Among hematopoietic cells, only αβ T cells showed consistent albeit low TOM expression in almost all tissues (Fig. 1E, ii). MR1 expression by double-positive (CD4$^+$CD8$^+$) thymocytes sustains MAIT cell development (*10*, *30*). We observed similar TOM expression in these and other thymocyte populations, with higher levels in mature CD4$^+$ and CD8$^+$ conventional T cells and regulatory T cells (Fig. 1F). Some B cells (B-1 but not B-2 cells), expressed TOM in the thymus and the peritoneal cavity (PerC) [Fig. 1, E ii and G]. Among myeloid cells, those that expressed TOM were mast cells in the PerC and skin; dendritic cells (DCs) in the thymus and skin; and MΦ in multiple tissues. The cells that expressed the highest levels of TOM in the entire animal were MΦ in the lungs, the pleural cavity, and the PerC (Fig. 1E, ii).

MΦ can be subdivided into two major subsets. The first are those derived from embryonic yolk sac and liver precursors and are self-renewing (*31*). These are replaced over time by the second subset, MΦ derived from bone marrow monocytes (*31*), at a rate that varies among tissues. For example, large peritoneal MΦ (LPMΦ) and AMΦ of the PerC and lungs, respectively, are replaced very slowly or not at all (*32*–*34*), whereas small peritoneal MΦ (SPMΦ) and lung interstitial MΦ (IMΦ) are replaced more rapidly (*34*, *35*). LPMΦ and AMΦ expressed high levels of TOM, whereas SPMΦ and IMΦ showed no or little TOM expression (Fig. 1, H and I). Hematopoietic cells of male and female mice expressed similar levels of TOM (fig. S3).

For the nonhematopoietic cells, TOM expression was identified in lung, salivary gland, bladder, vagina, and skin (Fig. 1E, i). In lymph nodes, TOM expression was low (Fig. 1E, i) but detectable in lymphatic and blood endothelial cells (fig. S4A). The cells with the highest levels of TOM in lungs and skin were bronchial epithelial cells and keratinocytes, respectively (fig. S4, B and C). MR1-expressing cells were thus generally located at the key microbial-facing layers and vasculature of various tissues.

We measured MR1 protein expression in single-cell suspensions isolated from PerC, lungs, spleen, liver, and small intestine of *Mr1*^{WT} or *Mr1*^{KO} (negative control) mice, after incubation in vitro with MR1 ligand, JYM87. The pattern of MR1 protein levels correlated well with that of TOM expression in *Mr1*^{TOM} mice, with macrophages showing the highest levels (Fig. 1J). The exception was B-1 cells of the PerC and IMΦ, which displayed a higher level of MR1 protein than that of LPMΦ and AMΦ, which was not predicted by TOM expression (Fig. 1, H and I). This may be because a higher level of autofluorescence in LPMΦ and AMΦ "masks" the actual level of MR1 expression, or because the degradation rate of TOM in B-1 cells of the PerC and IMΦ was lower than in other cells.

We also treated single-cell suspensions isolated from lungs, spleen, and blood of healthy human organ donors with JYM87 (fig. S5A). These analyses revealed an expression pattern similar to what we observed in mice, with the highest level of MR1 expression detected in AMΦ followed by IMΦ (Fig. 1K and fig. S5B). These results were also in agreement with an independent human single-cell RNA-sequencing (scRNA-seq) dataset (fig. S5C) (*36*, *37*). On the basis of our data, we concluded that mouse and human MΦ of various tissues, notably the lungs, were the cells that expressed the highest level of MR1.

Macrophages efficiently capture and present extracellular MR1 ligands

To determine whether the level of MR1 expression in different cells correlated with the relative capacity of those cells to capture MR1 ligands, we used a MR1 antigen analog labeled with cyanine5 (MAgA-Cy5) (*29*) as a tracker. Measurements of MAgA-Cy5 uptake in vitro by the 18 cell types that we analyzed in Fig. 1J showed that PerC LPMΦ and SPMΦ, and lung AMΦ, were 10-fold more effective than other cell types at capturing the ligand (Fig. 2A). We also compared the capacity of multiple cell types of the PerC, the lungs, and the spleen to present in vitro titrated amounts of the VitBAg, 5-OP-RU, to Bw58.MAIT cells (*38*). Bw58.MAIT cells express a MAIT TCR and up-regulate CD137 expression upon recognition of MR1–5-OP-RU complexes on the surface of APC. PerC, LPMΦ, and lung AMΦ were ~100 to 1000 times more efficient than any other cell type analyzed at stimulating Bw58.MAIT cells (Fig. 2B). Only PerC B-1 cells and, to a much lower extent, splenic DCs demonstrated detectable MR1 antigen presentation capacity. The scarcity of PerC SPMΦ and DCs—and of lung IMΦ, monocytes, neutrophils, and eosinophils—prevented us from analyzing these cell types on their own. A preparation of lung CD11b$^+$ cells that excluded MΦ (fig. S6) failed to present 5-OP-RU above the level of detection.

To examine which cells were more efficient at capturing and presenting MR1 ligands in vivo, we administered MAgA-Cy5 intranasally or intraperitoneally to *Mr1*^{TOM} reporter mice. The TOM$^+$ cells of the lungs and PerC, respectively, were more efficient than TOM$^-$ cells at capturing MAgA-Cy5 (Fig. 2C). Even when administered intravenously, around half of the lung TOM$^+$ cells, but none of their TOM$^-$ counterparts, captured the ligand (Fig. 2C, ii).

PerC LPMΦ and lung AMΦ were the cells that captured the largest amount of MAgA-Cy5 administered intraperitoneally and intranasally, respectively (Fig. 2D, ii). Differences in MAgA-Cy5 capture among cell types might be due to an intrinsic capacity to uptake and/or to accumulate the ligand intracellularly. This might explain why poorly endocytic cells such as B or T cells remained MAgA-Cy5–negative (Fig. 2D, ii). Another cause for differential uptake might be anatomical access to the ligand. For example, ligand provided by the intranasal route would be more accessible to AMΦ, which patrol the inner layer of alveoli, than to IMΦ, which reside in lung tissue. However, given that the cells that captured the largest amount of ligand in vitro (Fig. 2A) and in vivo (Fig. 2D ii) were the same, it appeared that the intrinsic ability to capture ligands was the major contributor to differences among cell types. The cells that expressed the highest levels of MR1 (MΦ) were also the ones endowed with the highest capacity to capture MR1 ligands. However, MR1 expression was not required for capture or intracellular accumulation of ligands because MΦ of *Mr1*^{KO} mice retained their capacity to capture MAgA-Cy5 (Fig. 2D, ii).

In addition to uptake of MAgA-Cy5, its presentation at the cell surface could be detected with an antibody against Cy5 (Fig. 2E, i). Cell-surface presentation of MAgA-Cy5 could be detected on LPMΦ and B-1 cells of the PerC and on lung AMΦ and endothelial cells (Fig. 2E, ii).

On the basis of the results of MR1 expression, ligand capture, and presentation, we concluded that PerC LPMΦ and lung AMΦ were the only cell types that consistently and unambiguously demonstrated the highest capacity for MR1 VitBAg presentation.

MR1 expression is influenced by the tissue environment and microbiota

The MΦ subtypes that are derived from fetal precursors and predominantly renew in situ (AMΦ and LPMΦ) (*31*–*34*) expressed higher levels of MR1 than those constitutively replenished from monocyte precursors (IMΦ and SPMΦ) (Fig. 1, H and I). These differences might be caused by cell-intrinsic mechanisms promoting MR1 expression that are active only in MΦ derived from fetal precursors. Alternatively, MR1 expression may be induced by environmental factors present in the tissue niches in which fetal-derived AMΦ and LPMΦ differentiate (*33*).

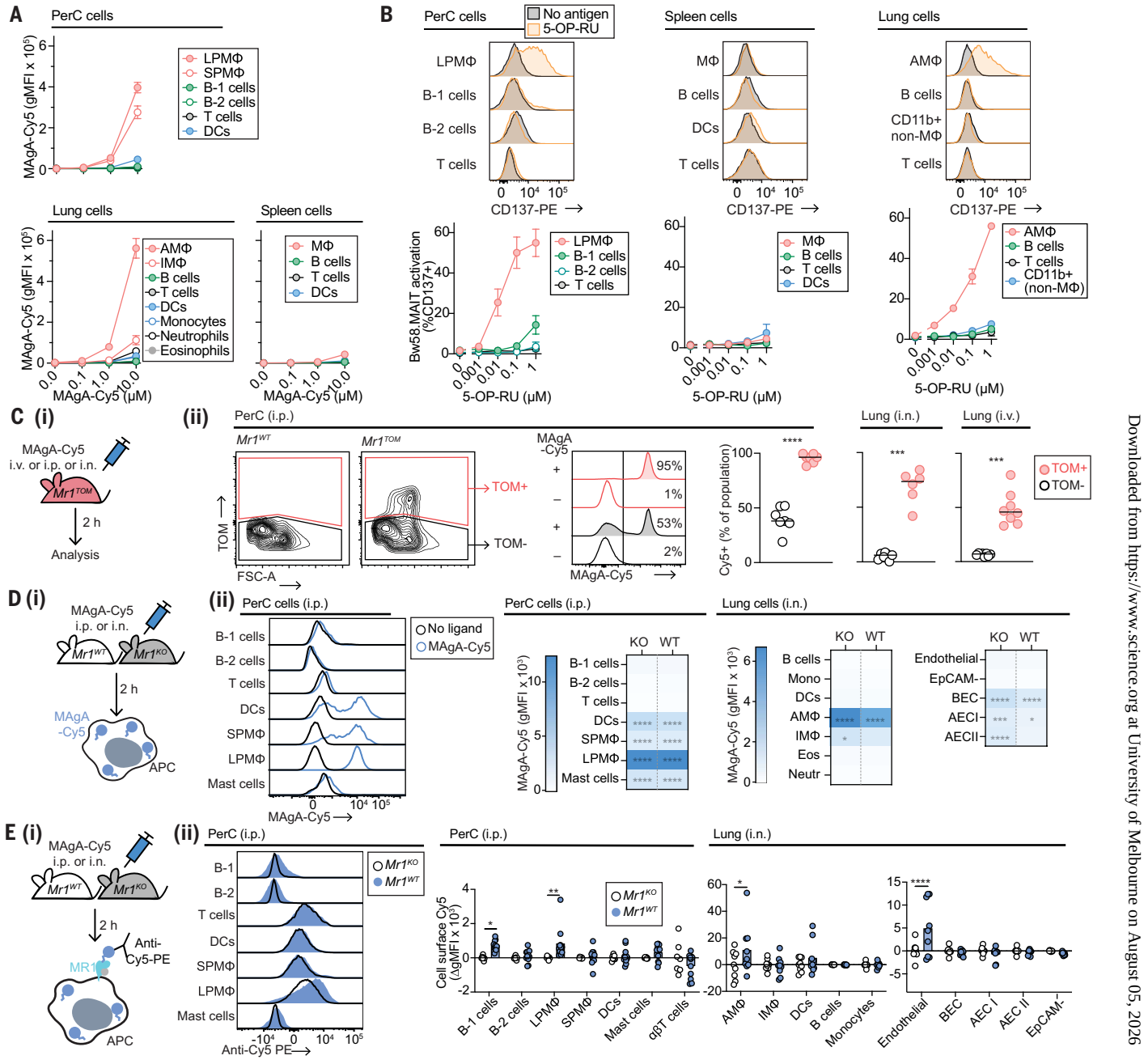

Fig. 2. Macrophages can efficiently capture extracellular Ag for presentation by MR1. (**A**) Cells isolated from the indicated tissues of *Mr1*^{WT} mice were cocultured with or without the indicated amounts of MAgA-Cy5 (0.1 to 10 μM) for 2 hours then analyzed for gMFI of Cy5 by means of flow cytometry. (**B**) The indicated cell types were sorted from *Mr1*^{WT} mice and cocultured with Bw58.MAIT cells for 16 hours in the presence or absence of the indicated amounts of 5-OP-RU (0.001 to 1 μM). Bw58.MAIT cell activation was measured by use of the surface activation marker CD137; representative flow cytometry histograms and the proportion of CD137$^+$ cells are shown. (**C**) (i) Schematic for administration of WT C57BL/6J or *Mr1*^{TOM} mice with 2 nmol MAgA-Cy5 through intraperitoneal, intranasal, or intravenous routes. (ii) After 2 hours, the frequency of Cy5$^+$ cells was assessed in either the TOM$^+$ or TOM$^-$ fraction of live cells from the PerC (intraperitoneal administration) or lungs (intranasal and intravenous administration). (**D**) (i) Schematic for detection of cells that uptake MAgA-Cy5. (ii) *Mr1*^{WT} or *Mr1*^{KO} mice was administered MAgA-Cy5 (2 nmol) intraperitoneally or intranasally, and cells were analyzed after 2 hours for gMFI of Cy5 by means of flow cytometry. (**E**) (i) Schematic for detection of cells that present cell-surface MAgA-Cy5. (ii) *Mr1*^{WT} or *Mr1*^{KO} mice were administered MAgA-Cy5 as in (D). Cell-surface MAgA-Cy5 was detected with an antibody to Cy5, and the signal from *Mr1*^{WT} mice was subtracted (ΔgMFI). Data are represented as the mean from two independent experiments [(A) and (B), $n = 8$ mice] or the mean from at least two independent experiments [(C) to (E), $n = 7$ to 11 mice]. [(C) and (E)] Dots indicate individual mice, and [(B) to (E)] representative flow cytometry histograms are shown. Gating strategies for lung, PerC, and spleen were identical to those shown in fig. S2, A to C, except that markers occupying the Cy5 channel were measured by using an alternative fluorochrome. Statistical significance was calculated by using (C) an unpaired Student's *t* test or [(D) to (E)] two-way ANOVA followed by a multiple comparison test where $^*P < 0.05$, $^{**}P < 0.01$, $^{***}P < 0.001$, and $^{****}P < 0.0001$.

Monocyte precursors of MΦ lacked MR1 expression (Fig. 3A). We reasoned that if MR1 expression were controlled by cell-intrinsic mechanisms, replacement of fetal AMΦ and LPMΦ with monocyte-derived MΦ would lead to formation of new AMΦ and LPMΦ lacking MR1 expression. Alternatively, if MR1 expression were induced by local tissue factors, the monocyte-derived AMΦ and LPMΦ would express MR1 as their fetal-derived counterparts did. We irradiated *Mr1*^{WT} and *Mr1*^{TOM} mice to eliminate the majority of embryonic tissue-resident MΦ and then transferred bone marrow of the reciprocal phenotype to reconstitute the MΦ populations from monocyte precursors (Fig. 3B i). After 2 months, most MΦ were derived from the donor monocytes, as determined by their congenic markers (Fig. 3B ii). The MΦ derived from *Mr1*^{WT} monocytes lacked TOM expression as expected (Fig. 3C). The AMΦ and LPMΦ derived from *Mr1*^{TOM} monocytes expressed TOM, whereas their IMΦ and SPMΦ counterparts did not, recapitulating the pattern observed in normal (nonchimeric) *Mr1*^{TOM} animals (Fig. 3C). This implied that MR1 expression was not dictated by the origin of the MΦ but by local factors that induced MR1 expression only in the tissue niches where AMΦ and LPMΦ developed.

The microbiota is essential for MAIT cell development because germ-free (GF) mice lack detectable MAIT cells in peripheral tissues (fig. S7A) (*10*, *26*, *39*). We hypothesized that the microbiota may contribute to local regulation of MR1 expression. We found that MR1 protein levels in PerC MΦ of mice maintained in GF conditions was lower than in cells isolated from mice bred in a specific pathogen–free (SPF) facility (fig. S7B). To characterize more extensively how the lack of microbiota affected MR1 expression in different tissues, we bred *Mr1*^{TOM} mice in GF conditions and compared the pattern of TOM expression with that in SPF *Mr1*^{TOM} mice. Most cell types expressed similar levels of TOM, but GF LPMΦ and to a lesser extent AMΦ and αβT cells of the small intestine had lower TOM expression than their SPF counterparts did (Fig. 3D). TOM expression was increased in LPMΦ, but not in AMΦ, through colonization of GF mice with SPF microbiota (Fig. 3E). The PerC is exposed to diverse and abundant products of the microbiota (*40*), more so than the skin and the lungs (*41*); this may explain why GF conditions had a higher influence on MR1 expression in the PerC.

We also assessed the effect of exposing SPF mice to a "wilder" microbiome by cohousing them with a microbially diverse or "dirty" mouse line [JaCa mice (*42*)]. After 30 days of exposure, both the fecal and the lung microbiomes increased in diversity, adapting to those of dirty mice (fig. S7C). In the dirty-cohoused *Mr1*^{WT} mice, MR1 surface levels increased in AMΦ and B-1 cells (Fig. 3F) but not in other cells

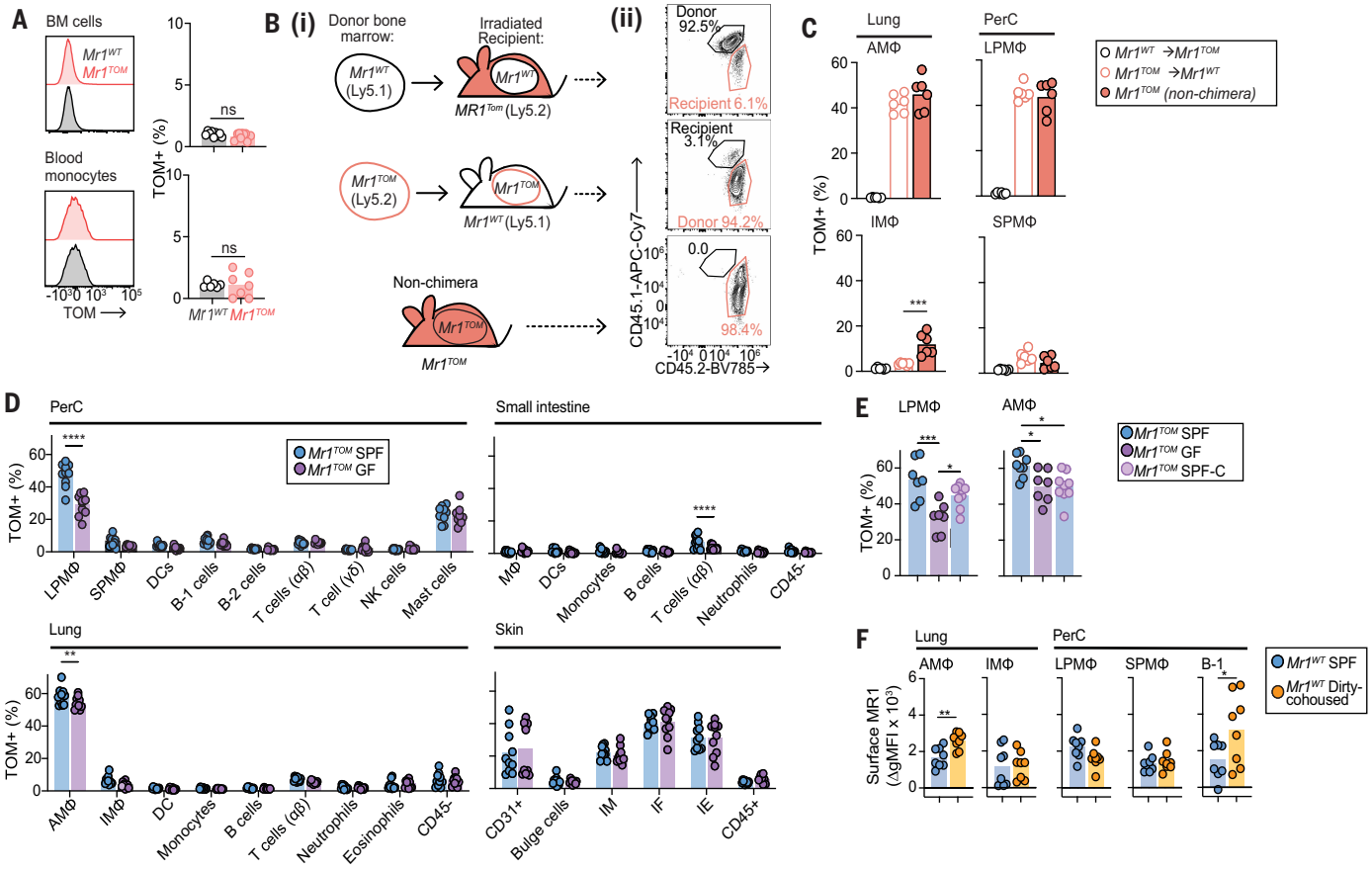

Fig. 3. Tissue environment and microbiota influences MR1 expression. (**A**) TOM expression in bone marrow (BM) cells or blood monocytes from *Mr1*^{WT} and *Mr1*^{TOM} mice. (**B**) (i) Schematic for BM chimera experiment. (ii) Donor and recipient MΦ identified by expression of congenic markers Ly5.1 and Ly5.2. Shown are AMΦ from lungs. (**C**) TOM expression among subsets of MΦ from the lungs (AMΦ or IMΦ) or PerC (LPMΦ or SPMΦ) derived from the indicated BM in chimeric animals, or in *Mr1*^{TOM} mice. (**D**) TOM expression among cells of the PerC, small intestine, lung, or ear skin from *Mr1*^{TOM} mice housed under SPF and GF facilities. (**E**) TOM expression among LPMΦ or AMΦ from SPF or GF facilities, or GF mice colonized with SPF flora (SPF-C). (**F**) Up-regulated MR1 protein level (ΔgMFI) after 3 hours in vitro culture with the MR1 ligand JYM87 (10 μM), in the indicated cell populations of *Mr1*^{WT} mice under SPF conditions or after cohousing with dirty (JaCa) mice for more than 30 days. Bars indicate the mean from two independent experiments, dots indicate individual mice [(A), $n = 7$ to 9; (C), $n = 6$; (D), $n = 10$; (E), $n = 7$ to 9; and (F), $n = 8$], and representative flow cytometry plots are shown [(A) and (B)]. Gating strategies for lung, PerC, and small intestine were identical to those shown in fig. S2, and gating strategy for skin was identical to fig. S4B. Statistical significance was calculated by using [(A) and (F)] an unpaired Student's *t* test, [(C) and (E)] a one-way ANOVA, or (D) two-way ANOVA followed by a multiple comparison test where $*P < 0.05$, $**P < 0.01$, $***P < 0.001$, and $****P < 0.0001$, or not significant (n.s.).

examined. These results indicated that higher abundance and/or diversity of the microbiota induced MR1 expression, especially in cells most exposed to commensal microbes or their products.

Cell type–specific gene regulation of *Mr1*

To gain insights into the regulation of *Mr1* transcription and the impact of the microbiota, we performed ATAC-seq (assay for transposase-accessible chromatin with high-throughput sequencing) (*43*) on AMΦ, LPMΦ, and B-2 cells isolated from GF mice that had been colonized with SPF microbiota (SPF-C) and LPMΦ isolated from GF mice. These cells were chosen for their varying MR1 expression (as indicated in Fig. 4A, i). All MΦ had five distinct regions of open chromatin ("peaks") in *Mr1*, whereas in B-2 cells, only peaks 2 to 4 were present (Fig. 4A, i and ii). Peak 2 includes the predicted *Mr1* promoter region (*44*). Because peaks 1 and 5 were only accessible in MΦ, they likely represented enhancer regions that allow *Mr1* expression (Fig. 4A, i and ii). There was no difference in peaks between GF and SPF-C LPMΦ, suggesting that the effect of the microbiota on MR1 expression (fig. S7B) was not caused by changes in gene accessibility (Fig. 4A).

We compared the transcriptomes of GF and SPF-C LPMΦ by means of RNA-sequencing (RNA-seq). There were 316 genes up-regulated in SPF-C LPMΦ (Fig. 4B). The predominant gene pathways enriched after microbiota colonization were the cholesterol biosynthesis pathway (for example, represented by *Cd36*, *Lpl*, and *Ldlr*) and those associated with innate signaling such as through Toll-like receptors (TLRs) and interferons (for example, *Nfkb2*, *Relb*, *IRF1*, *IRF4*, *Stat2*, *TNF*, *Nod2*, *Oasl2*, *Mx1*, and *Cd86*). This suggested that LPMΦ received microbiota signals through TLR detection of pathogen-associated molecular patterns (PAMPs) and type I interferons (*46*).

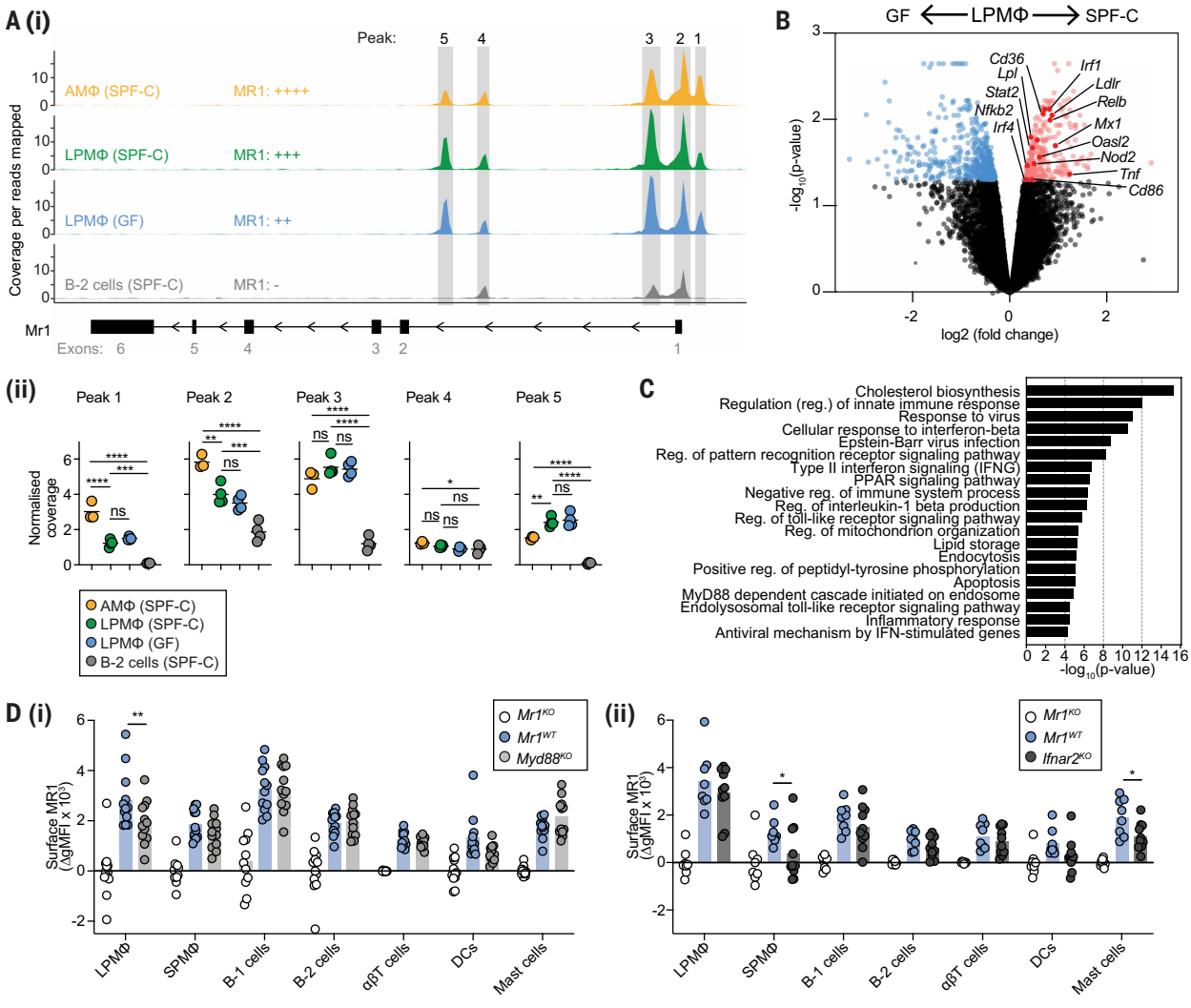

Fig. 4. Regulation of MR1 expression. (**A**) (i) Accessibility of the *Mr1* gene (determined with ATAC-seq) in AMΦ, LPMΦ, or B-2 cells from $Mr1^{WT}$ mice housed in SPF-C or GF conditions. The relative MR1 expression level is indicated with plus or minus symbols. (Bottom) Schematic of *Mr1* gene structure, with numbered exons in gray. Major peaks are numbered in the direction of gene transcription. (ii) Normalized coverage (log_{10}) of each peak from (i). (**B**) RNA-seq data represented in a volcano plot showing differentially expressed genes between LPMΦ from SPF-C or GF mice. Those in red are up-regulated and in blue are down-regulated in SPF-C mice. (**C**) List of the top 20 gene pathways enriched in LPMΦ of SPF-C mice compared to LPMΦ of GF mice. (**D**) Up-regulated MR1 protein level (ΔgMFI) after 3 hours in vitro culture with the MR1 ligand JYM87 (10 μM), in the indicated PerC cell populations from (i) $Mr1^{WT}$, $MyD88^{KO}$ or (ii) $Ifnar2^{KO}$ mice. Dots in (A) indicate biological replicates each from separate pooled mouse samples ($n = 4$ mice pools). Dots in (D) indicate individual mouse, and bars indicate the mean from at least two independent experiments ($n = 8$ to 12 mice). The gating strategy for PerC was identical to fig. S2B. Statistical significance was calculated by using [(A) and (D)] one-way ANOVA followed by a multiple comparison test or (B) unpaired Students *t* test where $*P < 0.05$, $**P < 0.01$, $***P < 0.001$, and $****P < 0.0001$, or not significant (n.s.).

To test the role of these pathways on MR1 expression, we examined mice in which all cells were deficient in the signaling molecule Myd88 (*Myd88*^{KO}) that cannot receive signals through the majority of TLRs, nor the interleukin-1 (IL-1) and IL-18 receptors, or mice in which all cells were deficient in the interferon-α/β receptor α chain (*Ifnar2*^{KO}) that cannot respond to interferon signaling. MR1 expression was reduced in LPMΦ from *Myd88*^{KO} but not *Ifnar2*^{KO} mice (Fig. 4D). Mutant SPMΦ had normal MR1 expression (Fig. 4D, i), suggesting that MYD88 signaling only affected MR1 expression in MΦ exposed to the microbiome. MR1 expression in lung MΦ was not affected by the lack of MYD88 signaling (fig. S7D). We concluded that *Mr1* gene expression was regulated by DNA accessibility and by signals received by TLR ligands derived from the microbiota.

MΦ MR1-Ag presentation controls the composition and metabolism of the microbiota

Although our data indicated that MΦ may be the dominant MR1 APC, other cell types also expressed MR1 (Fig. 1). To test whether MR1 expression by MΦ was essential for MAIT cell activity in vivo, we generated a conditional MR1 knockout strain by crossing *Mr1*$^{f/f}$ (*10*) and *Lyz2*^{Cre} (LysM^{Cre}) mice (*45*). The *Lyz2* gene is expressed in MΦ, DC, monocytes, and granulocytes (*45*), so MR1 expression was lost in these cell types but not in B or T cells (Fig. 5A and fig. S8A).

Single-cell suspensions from the lungs, PerC, and spleen of *Lyz2*$^{Cre/+}$-*Mr1*$^{f/f}$ mice had a reduced ability compared with those from *Mr1*$^{f/f}$ to stimulate Bw58.MAIT cells in the presence of 5-OP-RU (fig. S8B). Because MΦ expressed much higher levels and are orders of magnitude more efficient at capturing and presenting MR1 ligands (Figs. 1 and 2) than are DCs, monocytes, or granulocytes, we attributed any impact on MR1-dependent biological activities in *Lyz2*$^{Cre/+}$-*Mr1*$^{f/f}$ mice to the loss of MR1 from MΦ, although we cannot formally discard a partial contribution by other MR1^{+} cells.

The number of MAIT cells in the lungs and PerC was unaffected in the mutant mice (Fig. 5B), as was the proportion of MAIT17 (RORγt^{+}) and MAIT1 (T-bet^{+}) subsets (fig. S8C) (*14*). This confirmed that MR1-expressing MΦ were not required for MAIT cell development, homeostatic maintenance, or subset imprinting in tissues. However, when 5-OP-RU was administered intravenously into *Lyz2*$^{Cre/+}$-*Mr1*$^{f/f}$ mice, lung and PerC MAIT cells failed to up-regulate CD69 to the level observed in *Mr1*$^{f/f}$ littermates, indicating that they were poorly activated (Fig. 5C). We concluded that MΦ played a key role in presentation of extracellular VitBAg.

MAIT cells reportedly recognize VitBAg produced by commensal bacteria (*4*, *47*) that colonize mucosal surfaces and contribute to shaping the composition of the microbiota (*11*, *48*). To test whether MR1 Ag presentation by MΦ was involved in this activity, we compared the gut, lung, and skin microbiomes of *Mr1*$^{f/f}$ and *Lyz2*$^{Cre/+}$-*MR1*$^{f/f}$ littermates and also *Mr1*^{KO} mice after cohousing for 2 weeks. Supervised machine learning [using partial least squares discriminant analysis (*49*)] revealed differences in the composition of the gut, skin, and respiratory microbiota between mouse strains (Fig. 5D). Deletion of MR1 did not affect within-sample (alpha) diversity in any site, as measured with either Faith's phylogenetic diversity, which captures the total evolutionary breadth of taxa in a sample, or Shannon diversity, which reflects both species richness (the number of taxa present) and evenness (the uniformity of their relative abundances) (fig. S9, A and B). *Mr1*^{KO} mice had distinct fecal, ear, and to a lesser extent lung microbiomes compared with those of *Mr1*$^{f/f}$ mice (Fig. 5D). By contrast, the biggest difference in the microbiome of *Lyz2*$^{Cre/+}$-*Mr1*$^{f/f}$ mice compared with those of *Mr1*^{KO} or *Mr1*$^{f/f}$ mice was observed in the lung, with little or no differences in feces and the skin (Fig. 5D). Because the *Mr1*^{KO} mice were not littermates with the *Mr1*$^{f/f}$ or *Lyz2*$^{Cre/+}$-*MR1*$^{f/f}$ mice, the differences in *Mr1*^{KO} mice to other strains may be due to incomplete normalization from cohousing (*50*). However, the *Mr1*$^{f/f}$ and *Lyz2*$^{Cre/+}$-*MR1*$^{f/f}$ mice were littermates, so we attributed these differences to the lack of MR1 expression in the conditional knockout mice, although there could be some contribution from expression of the Cre recombinase too.

To understand the species-level differences between the *Lyz2*$^{Cre/+}$-*Mr1*$^{f/f}$ and *Mr1*$^{f/f}$ littermates, we performed an ANCOM-BC2 analysis (*51*). This indicated that the microbiomes of the two mouse groups differed only in the lungs, with enrichment in two genera of bacteria, *Parabacteroides* and *Prevotella*, and depletion of *Corynebacterium*, in *Lyz2*$^{Cre/+}$-*Mr1*$^{f/f}$ mice (Fig. 5E). We did not observe a correlation between the abundance of specific microbes and their ability to synthesize riboflavin.

Changes in bacterial species can alter the metabolic balance of the microbiota (*52*). The differences in microbiome composition we observed in *Lyz2*$^{Cre/+}$-*Mr1*$^{f/f}$ and *Mr1*^{KO} mice compared with normal *Mr1*$^{f/f}$ mice predicted multiple metabolic pathway alterations in *Lyz2*$^{Cre/+}$-*Mr1*$^{f/f}$ and *Mr1*^{KO}, respectively (Fig. 5F and fig. S9C). The greatest pathway enrichments were observed in the lung microbiomes of *Lyz2*$^{Cre/+}$-*Mr1*$^{f/f}$ mice (fig. S9C), suggesting that MR1 Ag presentation by *Lyz2*-expressing cells played a more prominent role in the regulation of the microbiota in the lungs than in the gut or skin. The most different metabolic pathways were teichoic acid biosynthesis (part of the gram-positive bacterial envelope) and tyrosine biosynthesis (Fig. 5F).

We concluded that there was a form of reciprocal regulation between MR1 expression in macrophages and the microbiome. Because the microbiome of mice that lacked MR1 and MAIT cells was more altered than the microbiome of mice that had MAIT cells but lacked MR1 expression in *Lyz2*-expressing cells, it suggested that MAIT cells may regulate the microbiome using mechanisms both dependent and independent of MR1 recognition.

MR1 presentation by MΦ drives MAIT cell protection against infection

We examined the role of MR1 presentation by MΦ in host defense against bacterial pathogens. Intravenous infection of *Mr1*$^{f/f}$ mice with *Francisella tularensis* caused a reduction in the number of AMΦ and LPMΦ and an increase in the number of IMΦ, SPMΦ, and liver MΦ (fig. S10A). Similar changes were observed in *Lyz2*$^{Cre/+}$-*Mr1*$^{f/f}$ mice (fig. S10A). MR1 protein expression increased in IMΦ of infected C57BL/6J mice and did not change in the other cell types we examined (fig. S10B). Infection induced expansion of MAIT cells in the liver, spleen, lung, and PerC of *Mr1*$^{f/f}$ mice (Fig. 6A) (*14*), but little MAIT cell expansion was observed in their *Lyz2*$^{Cre/+}$-*Mr1*$^{f/f}$ counterparts (Fig. 6A). Because MAIT cells promote pathogen clearance (*13*, *14*, *17*), the bacterial burden in *Lyz2*$^{Cre/+}$-*Mr1*$^{f/f}$ mice was higher than in *Mr1*$^{f/f}$ mice, similar to that observed in infected *Mr1*^{KO} mice, where MAIT cells were completely absent (Fig. 6B). Similar defects in MAIT cell expansion and changes in AMΦ and IMΦ numbers were obtained after intranasal infection with the pulmonary pathogen *Legionella longbeachae* (Fig. 6C and fig. S10C). To test the role of B cells in MAIT cell expansion, we also infected B cell–deficient mice (μMT) with *L. longbeachae*; MAIT cells expanded normally in these mice (fig. S10D). These results supported the notion that MR1 antigen presentation by MΦ plays a critical role in the induction of protective MAIT cell responses against bacteria.

To test the possibility that MAIT cells were impaired in *Lyz2*$^{Cre/+}$-*Mr1*$^{f/f}$ mice and hence could not respond to bacterial infection even if non-MΦ were presenting antigens on MR1, we infected intranasally *Mr1*$^{f/f}$ and *Lyz2*$^{Cre/+}$-*Mr1*$^{f/f}$ littermates with *Salmonella enterica* serovar Typhimurium. This is an artificial model of ectopic infection because this pathogen normally infects the gut epithelium (*53*) but has been shown to trigger a MAIT cell response in the lungs driven by MR1 expressed by nonhematopoietic cells (*22*). MAIT cells expanded similarly in infected *Mr1*$^{f/f}$ and *Lyz2*$^{Cre/+}$-*Mr1*$^{f/f}$ mice (Fig. 6D). We concluded that the failure of MAIT cells to expand in *Lyz2*$^{Cre/+}$-*Mr1*$^{f/f}$ mice infected with *F. tularensis* (Fig. 6A) or *L. longbeachae* (Fig. 6B) was due to deficient MR1 antigen presentation.

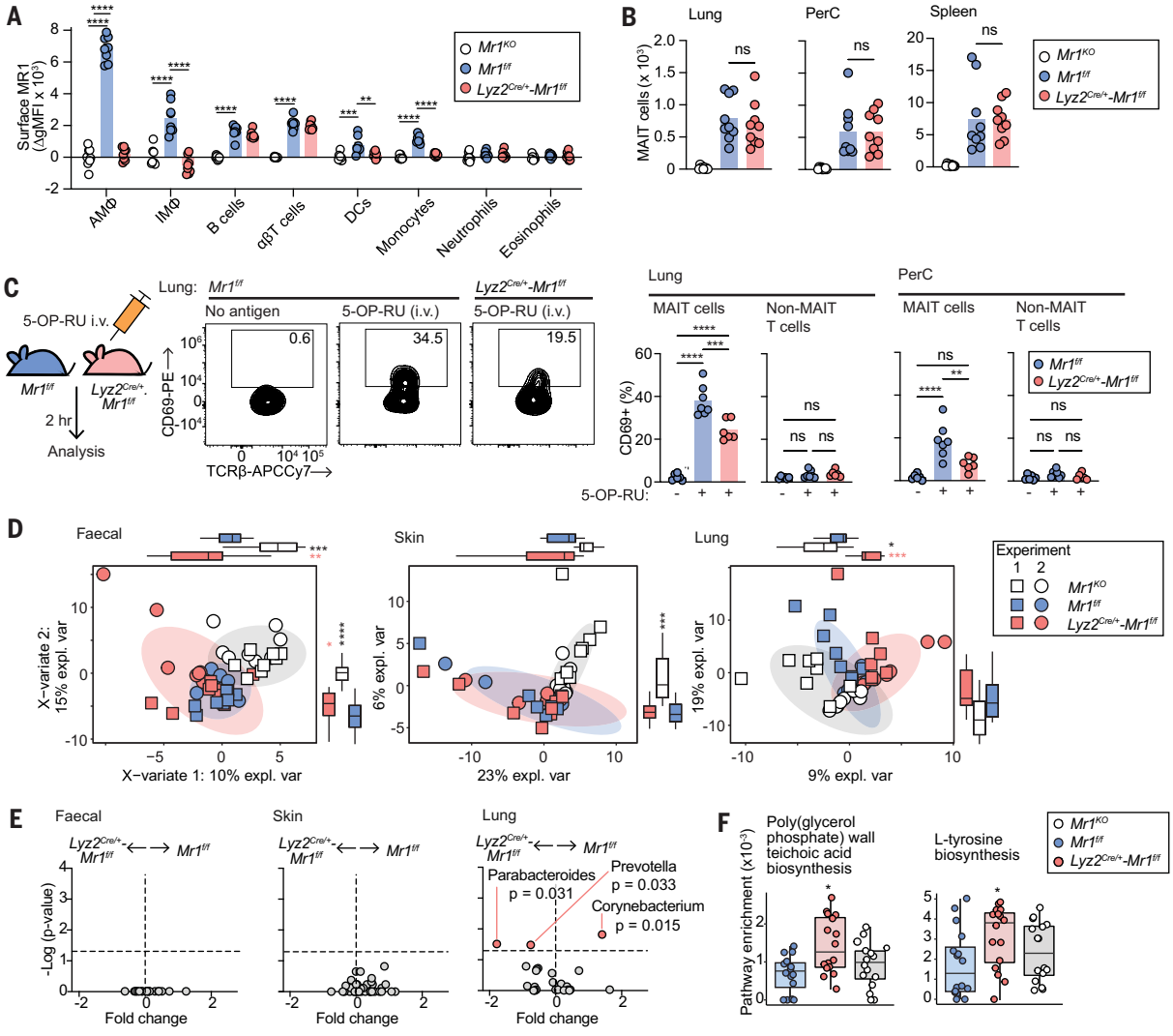

Fig. 5. Macrophage expression of MR1 drives MAIT cell modulation of the lung microbiome. (**A**) Up-regulated MR1 protein level (ΔgMFI) after 3 hours in vitro culture with the MR1 ligand JYM87 (10 μM), in the indicated cell populations from lungs of $Mr1^{f/f}$ or $Lyz2^{Cre/+}$-$Mr1^{f/f}$ mice. (**B**) Number of MAIT cells in lung, PerC, and spleen of the indicated mice. (**C**) Mice were injected intravenously with or without 5-OP-RU (100 pmol). The activation of MAIT or other αβ (non-MAIT) T cells was measured after 2 hours by means of flow cytometry and represented as the percentage of $CD69^+$ cells of the whole population. Example flow cytometry plots of lung MAIT cells are shown. (**D**) 16*S* ribosomal DNA (rDNA) microbiomes of fecal, skin, or lung samples from cohoused $Mr1^{KO}$, $Mr1^{f/f}$, or $Lyz2^{Cre/+}$-$Mr1^{f/f}$ mice compared by means of partial least squares discrimination analysis. The dispersion of each sample along the *x*-variates 1 and 2 are shown as box plots. Two independent experiments are indicated with shapes. (**E**) Species altered in $Lyz2^{Cre/+}$-$Mr1^{f/f}$ mice compared with $Mr1^{f/f}$ mice (where $P < 0.05$ indicates significantly altered taxa, indicated with red symbols). (**F**) The top metabolic pathways enriched in $Lyz2^{Cre/+}$-$Mr1^{f/f}$ mouse lung microbiomes inferred from 16*S* rDNA sequencing data and compared by means of ANOVA where the asterisks indicate Benjamini-Hochberg corrected $P < 0.2$. Bars indicate the mean from at least two pooled independent experiments, and dots indicate individual mice [(A), $n = 8$; (B), $n = 9$; and (C), $n = 7$]. Dots in (D), (E), and (F) indicate individual mice from two independent experiments ($n = 16$). Gating strategies for immune cell populations in (A) to (C) are shown in fig. S2. Statistical significance was calculated by using [(A) to (C) and (F)] one-way ANOVA followed by a multiple comparison test, (E) adjusted for multiple comparisons by using the Benjamini–Hochberg false discovery rate correction implemented in ANCOM-BC2, where $*P < 0.05$, $**P < 0.01$, $***P < 0.001$, and $****P < 0.0001$, or not significant (n.s.).

Discussion

MAIT cells are the most abundant (*54*) members of a wider family of T lymphocytes that recognize Ags presented by MR1 known as MR1T cells (*25*). MAIT cells recognize microbial antigens, but other MR1T cells recognize tumor and normal self Ags (*55*) and may protect against cancer (*56*) or contribute to autoimmiunity (*57*, *58*), respectively. Therapies that harness MR1 antigen presentation and MR1 T cell recognition might have widespread applications, and because MR1 is nearly monomorphic (*25*), they would be applicable across the entire human population. Development of such therapies requires characterization of the APCs that perform MR1 antigen presentation and their roles in health and disease. In this work, we showed that MΦ express the highest levels of MR1 in mice and humans in a range of tissues, including lungs, PerC, liver, and spleen. A notable exception is in the intestines, where MR1 was not detected in any cell type. Of the tissues examined, MΦ capture and present VitBAg with high efficiency and play a pivotal role in MAIT cell immunity, highlighting their potential as universal agents for MR1T cell immunotherapy.

MR1 expression is transcriptionally regulated, indicated by differences in *Mr1* gene accessibility in high-MR1-expressing (MΦ) versus low-MR1-expressing (B lymphocytes) cells. Yet-undescribed tissue factors also contribute to regulate *Mr1* transcription among MΦ

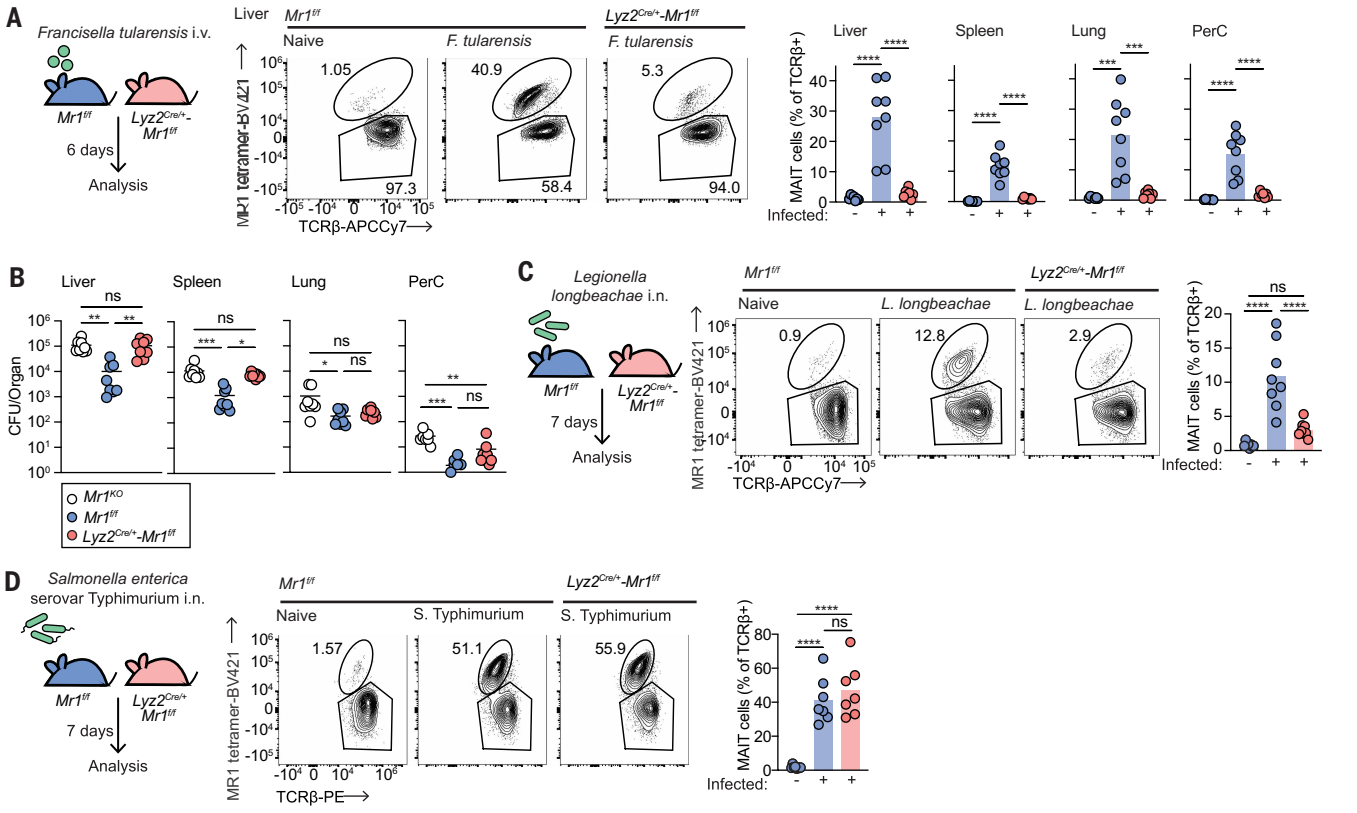

Fig. 6. Macrophage expression of MR1 drives MAIT cell responses during bacterial infection. (**A**) Mice were either uninfected or infected intravenously with 10^4 CFU *F. tularensis* live vaccine strain. MAIT cell frequency of αβ TCR$^+$ cells was assessed in liver, spleen, lung, and PerC at 6 days after infection. (**B**) *F. tularensis* bacterial loads from tissues of mice from (A) were enumerated and assessed at 6 days after infection. (**C**) Mice were either uninfected or infected intranasally with 10^4 CFU *L. longbeachae*, and MAIT cell frequencies of αβ TCR$^+$ cells were enumerated at 7 days after infection. (**D**) Mice were either uninfected or infected intranasally with 5×10^5 CFU *S. enterica* serovar Typhimurium, and MAIT cell frequencies of αβ TCR$^+$ cells were enumerated at 7 days after infection. Bars indicate the mean from two pooled independent experiments, dots indicate individual mice [(A) to (C), $n = 8$, and (D), $n = 7$], representative flow cytometry plots are shown [(A), (C), and (D)]. Gating strategy for MAIT cells was identical to fig. S2G. Statistical significance was calculated by using one-way ANOVA followed by a multiple comparison test where $^*P < 0.05$, $^{**}P < 0.01$, $^{***}P < 0.001$, and $^{****}P < 0.0001$, or not significant (n.s.).

populations that reside in different locations. Exposure to products of the local microbiota, likely through TLR signaling, fine tunes expression levels. The mechanisms that capture and transport VitBAg to the ER (*25*) may be regulated by the same factors that control MR1 expression, but this is speculative at present.

We showed that MΦ play a critical role in MR1 presentation and induction of antibacterial MAIT cell responses. They are not required for MAIT cell development in the thymus because this is driven by MR1-expressing thymocytes (*59*). They were also dispensable for maintenance of peripheral MAIT cells able to respond to VitBAg presented by other cells. This implies that MAIT cell homeostasis does not require MR1 expression by MΦ or that multiple cell types can fulfill this function. By contrast, lack of MR1 expression in MΦ altered the microbiota and potentially the metabolome, particularly in the lung, although the effect was not as pronounced as in mice that lack MR1 and MAIT cells entirely (*11*). We observed an inverse correlation between the level of MR1 expression and the level of exposure to commensal flora in MΦ from different locations. For example, MR1 was expressed by MΦ in the lungs and the spleen, which are largely sterile, but not by MΦ in the gut, where commensal bacteria are abundant. MR1 expression may thus be fine tuned to ensure that sufficient MR1 ligands are presented to MAIT cells at locations where the source of VitBAg is scarce, while preventing potentially deleterious activation of MAIT cells at locations where commensal bacteria produce high levels of VitBAg. Collectively, our results suggest that MR1 antigen presentation by MΦ might be therapeutically manipulated to reverse dysbiosis (*60*).

The mouse strain that we used to eliminate MR1 expression in MΦ (*Lyz2$^{Cre/+}$-Mr1$^{f/f}$*) also affected expression in DC and monocytes. It is possible that these two cell types contributed to MAIT cell recruitment against *F. tullarensis* and *L. longbechae*. However, the greater level of MR1 expression in MΦ before or during infection, and that MΦ were constitutively able to capture and present MR1 ligands orders of magnitude more efficiently than other cell types we examined, argued against this possibility. However, we cannot discard the possibility that other immune cells may play a more prominent role in other immune responses mediated by MR1.

Our findings implicated MΦ as a prominent MR1 APC. They contributed to regulation of the microbiome, presumably by presenting commensal ligands, and induced MAIT cell immunity against bacterial infection. MΦ have also been shown to influence antitumor MAIT cell responses (*56*). MΦ therefore emerged as central agents for MR1 Ag presentation and regulation of immunity by MAIT and, potentially, other MR1T cell subsets.

Materials and methods

Ethics

All animal experiments were approved by the University of Melbourne Ethics Committee (#21308 and #1714375) and conducted in accordance with the National Health and Medical Research Council Australian

Code of Practice for the Care and Use of Animals for Scientific Purposes. Human tissue samples were obtained from deceased organ donors at the time of organ collection for transplantation through the Australian Donation and Transplant Biobank (*61*) with ethics approval from the University of Melbourne Human Research and Ethics Committee (#2024-20462-49563-7). Buffy coats from healthy human donors were obtained from the Australia Red Cross Lifeblood Service with written and informed consent and with ethics approval from the University of Melbourne Human Research and Ethics Committee (#2024-21201-49519-5).

Mice

The *Mr1-tdTomato* ($Mr1^{TOM}$) reporter mice were generated by inserting the *tdTomato* coding sequence in-frame immediately following the ATG start codon of the *Mr1* gene. This was performed by the MAGEC laboratory as previously reported (*62*), complying with relevant ethical regulations and approved by the Walter and Eliza Hall Institute (WEHI) Animal Ethics Committee. Briefly, 20 ng/μl of Cas9 mRNA, 10 ng/μl of sgRNA (targeting the insertion site) and 6 ng/μl of the targeting vector (containing the tdTomato coding sequence and flanked by homology arms) were injected into the pronucleus of fertilized one-cell stage embryos generated from wild-type C57BL/6J breeders. Twenty-four hours later, two-cell stage embryos were transferred into the uteri of pseudo-pregnant female mice. Targeted animals were backcrossed to wild-type C57BL/6J mice for four generations. All mouse strains were bred and maintained in specific pathogen–free conditions at the Bio21 Molecular Science and Biotechnology Institute. Experiments were performed on 6–13-week-old mice without gender preference in accordance with the Institutional Animal Care and Use Committee guidelines of the University of Melbourne.

The $Mr1^{f/f}$ mouse line was generated by Prof. Yasmine Belkaid and Dr. Michael Constantinides as described previously (*10*).

Germ-free (GF) mice [C57BL/6J ($Mr1^{WT}$) and $Mr1^{TOM}$)] were bred and maintained at the Translational Research Institute Gnotobiotic Facility (Brisbane, Queensland). Colonisation of GF mice without gender preference with SPF microbiota was achieved administering JAX normal flora by oral gavage twice, one week apart when mice were 8 and 9 weeks old. After 4 weeks the mice were culled for analysis and compared to germ-free littermates.

The microbially diverse or dirty mouse line, James Cagney (JaCa) mice, are described elsewhere (*42*). Briefly, the line was generated by Tri Giang Phan (Garvan Institute of Medical Research) and Jenny Kingham (Australian BioResources) with approval from the Garvan Institute of Medical Research/St Vincent's Animal Ethics Committee (#17_16 and 20_19). Outbred wildtype mice were obtained from a public educational farm (Calmsley Hill City Farm). The initial breeding pairs for the colony were treated with a topical application of Ivermectin (1 g/ml) and from 24 hours after this a continuous treatment with Fenbendazole (150 ppm) medicated feed to remove parasites. Sentinel mice were used to monitor mouse hepatitis virus, parvovirus, minute virus of mice, norovirus, Theiler's encephalomyelitis virus and rotavirus by serology every six months, and for *Helicobacter* by means of polyermase chain reaction (PCR) on pooled faeces. For cohousing experiments, JaCa female mice (>10 weeks old) were cohoused with 10-week-old female $Mr1^{WT}$ for >30 days for horizontal transmission of the microbiota and compared to age-matched female mice from standard SPF facilities.

Tissue processing for flow cytometry

Mice were humanly euthanized using CO_2. After cardiac perfusion with 10 ml PBS, tissues were extracted then diced finely. Tissues (apart from exceptions below) were digested with Liberase TL (0.25 mg/ml; Roche) and DNase (5 μg/ml; Roche) dissolved in Hank's balanced salt solution (HBSS) for 60 min at 37°C with occasional mixing. The digestion was passed through a 1 ml pipette tip 20 times and then passed through 70 μm mesh. Cells were washed and red blood cells (RBC) lysed were stained. Spleens were forced through 70 μm strainer, followed by RBC lysis. Blood was collected into a sodium heparin tube and then RBC lysed. Peritoneal and pleural cavity cells were collected by lavage using 5 ml ice-cold PBS with 5 mM EDTA and a 26G needle which was recovered after gentle agitation of the cavities. Livers were forced through 70 μm strainer, cells then isolated from debris using a 33% percoll gradient, followed by RBC lysis. Small and large intestines were processed with DTT-EDTA solutions (HBSS+5% FCS+10 mM HEPES+1 mM DTT+1 mM EDTA) for 30 min at 37°C with shaking at 230 rpm. Digested samples were then vortexed for at least 60 s before being passed through 70 μm mesh. Lymph nodes were digested with collagenase (2 mg/ml; Roche), DNase (0.1 mg/ml; Roche) and Dispase (0.8 mg/ml; Roche) in RPMI 1640 medium with 2% FCS for 25 min at 37°C. Digested samples were pipetted up and down for 90 times for further digestion before passed through 70 μm mesh.

Human lung and spleen samples (2 g) were diced finely with a scalpel blade and then digested with collagenase type 3 (3.5 mg/ml; Worthington Biochemical) and DNase I (1 mg/ml) dissolved in RPMI 1640 medium with 1% FCS and disrupted in a GentleMACS "C" tube on a Octo Dissociator (Miltenyi) with heating cuffs, then shaking at 180 rpm for 1 hour at 37°C, and finally passed through a 70 μm mesh and RBC lysed prior to antibody staining. Human peripheral mononucleated cells (PBMC) were isolated from buffy coats using Ficoll Paque PLUS (Cytiva) according to the manufacturer's instructions.

MR1 ligands

MR1 ligands were added directly to the culture medium in vitro or diluted in PBS and injected in vivo by the indicated administration routes. The MR1 ligands were synthesized as previously reported: JYM87 (*29*) [also known as the ribityl-less ligand (*28*)], 5-OP-RU (*63*) and MAgA-Cy5 (*29*) were stored in DMSO, were synthesized as previously reported. 5-OP-RU is unstable in water and was used immediately after dilution into aqueous buffer.

Flow cytometry, tetramers and antibodies

For MR1 surface staining, cells were isolated from tissues and then incubated for 3 hours at 37°C in DMEM medium, 10% FCS with 10 μM JYM87 (*29*) to up-regulate cell surface MR1. Fc receptors were blocked with clone 2.4G2 hybridoma supernatant, then surface MR1 was detected with biotinylated clone 8F2.F9 (reported previously (*64*) and produced from the hybridoma at the WEHI Antibody Facility) at 9.5 μg/ml along with phenotyping antibodies. Cells were then incubated with streptavidin-PE (Cat# 405204, Biolegend, 1:200); For MR1 intracellular staining, cells were isolated from tissues and Fc receptors were blocked with clone 2.4G2 hybridoma supernatant. Cells were then fixed with 2% PFA before cell membrane permeabilized with 0.1% saponin. Intracellular staining with MR1-PE (Clone 8F2.F9, WEHI antibody facility, 1 mg/ml, 1:3200) diluted in FACS buffer contains 0.1% saponin and 5% of normal mouse serum. For cell surface Cy5 staining, cells were isolated from mice injected with MAgA-Cy5 via different administration routes. Fc receptors were blocked with clone 2.4G2 hybridoma supernatant, then surface Cy5 was detected with anti-Cy3/Cy5-biotin (Clone CY-96, Cat# C3117, Sigma, 1:400). Cells were then incubated with streptavidin-PE (Cat# 405204, Biolegend, 1:200). The anti-MR1 and anti-Cy5 staining was normalised by subtracting the background which is the mean gMFI of the equivalent $Mr1^{KO}$ cell population from the signal in each sample (termed the ΔgMFI). MAIT cells were detected as previously reported (*65*) with MR1-5-OP-RU and MR1-6-FP tetramers which were a kind gift from the McCluskey laboratory (Doherty Institute, Melbourne, Victoria). Flow cytometry was performed on the Cytoflex LX (Beckman Coulter), and data were analyzed with FlowJo software (FlowJo VX).

Antibodies against mouse CD45 (Clone 30-F11, Cat# 564225, BV786, RRID:AB_2716861 1:200), Ly6G (Clone 1A8, Cat# 563978, BUV395,

RRID:AB_2716852, 1:200), SiglecF (Clone E50-2440, Cat# 740557, BV650, RRID:AB_27402581:200), CD19 (Clone 1D3, Cat# 566411, BB700, RRID:AB_2744315, 1:200), TCRβ (Clone H57-597, Cat# 560656, APC-Cy7, RRID:AB_1727574, 1:200), CD4 (Clone GK1.5, Cat# 563790, BUV395, RRID:AB_2738426 1:200), CD8a (Clone 53-6.7, Cat# 612898, RRID:AB_2870186, 1:400), and CD43 (Clone S7, Cat# 563206, BV510, RRID: AB_273806, 1:200) were purchased from BD Biosciences. Antibodies against mouse MerTK (Clone 2B10C42, Cat# 151510, BV421, RRID: AB_2832533, 1:200), CD11b (Clone M1/70, Cat# 101263, BV510, RRID:AB_2629529, 1:800), CD11b (Clone M1/70, Cat# 101236, BV421, RRID:AB_11203704, 1:200), CD31 (Clone MEC13.3, Cat# 102534, APC-Cy7, RRID:AB_2860596, 1:200), CD64 (Clone X54-5/7.1, Cat# 139306, RRID:AB_11219391, APC, 1:200), gp38 (Clone 8.1.1, Cat# 127423, BV421, RRID:AB_2814017, 1:400), CD326 (Clone G8.8, Cat# 118219, PerCP-Cy5.5, RRID:AB_2098647, 1:400), Sca-1 (Clone D7, Cat# 108112, APC, RRID:AB_313349, 1:200), NK-1.1 (Clone PK136, Cat# 108729, AF700, RRID:AB_2074426, 1:200), Ly6C (Clone HK1.4, Cat# 128026, APC-Cy7, RRID:AB_10640120, 1:200), and CD137 (Clone 17B5, Cat# 106105, PE, RRID:AB_2205693, 1:200) were purchased from Biolegend. Antibodies against mouse CD11c (Clone N418, FITC, 1:1000), MHC-II (Clone M5/114, AF700, 1:600), CD24 (Clone M1/69, 1:400), CD44 (Clone IM7.81, FITC, 1:400), CD69 (Clone H1-2F3, PE, 1:200), CD117 (Clone ACK2, FITC, 1:400), F4/80 (Clone F4/80, AF647, 1:400), B220 (Clone RA3-6B2, AF647, 1:200), and TCRγδ (Clone GL3, FITC, 1:200) were purchased from the Walter & Eliza Hall Institute (Melbourne, Victoria).

Antibodies against human CD3 (Clone SP34-02, Cat# 557917, AF700, RRID:AB_396938, 1:100), CD11c (Clone B-ly6, Cat# 563404, BV650, RRID:AB_2732048, 1:50), CD16 (Clone 3G8, Cat# 612945, BUV496, RRID: AB_2870224, 1:100), CD19 (Clone HIB19, Cat# 560727, APC-H7, RRID:AB_1727437, 1:50), CD45 (Clone HI30, Cat# 563792, BUV395, RRID:AB_2869519, 1:100), CD169 (Clone 7-239, Cat# 565353, BB515, RRID: AB_2739204, 1:400), CD206 (Clone 19.2, Cat# 550889, APC, RRID: AB_398476, 1:50), and HLA-DR (Clone G46-4, Cat# 564041, BV786, RRID:AB_2738559, 1:200) were purchased from BD Biosciences.

Quantitative real-time PCR (qPCR)

Taqman gene expression assays (Life Technology) for mouse *MR1* (Assay ID: Mm00468487_m1), Glyceraldehyde 3-phosphate dehydrogenase gene *Gapdh* (Assay ID: Mm99999915_g1), Importin 8 gene *Ipo8* (Assay ID: Mm01255158_m1) were used for qPCR. 50,000 cells of each cell population were sorted into 100 µl RNA Lysis Buffer RLY and 2 µl tris (2-carboxyethyl) phosphine (TCEP) and RNA isolated using the Isolate II RNA Micro Kit (Bioline). cDNA was synthesized using SensiFAST cDNA Synthesis Kit (Bioline) according to the manufacturer's instructions. Pre-amplification was performed with the TaqMan PreAmp Master Mix and pooled TaqMan Gene Expression Assays according to the manufacturer's instructions. The qPCR was performed with TaqMan Fast Advanced Master Mix and TaqMan Gene Expression Assays and data acquired via QuantStudio 6 and 7 Flex Real-Time PCR Systems and Mr1 expression analyzed using the 2-ΔΔCT method relative to the average of both housekeeping genes *Gapdh* and *Ipo8*.

Ex vivo MR1 antigen presentation assay

BW5147.TCR $\alpha^-\beta^-$ thymoma cells expressing CD3 were transduced with a canonical murine MAIT cell TCR (TRBV13-2) as previously described (*38*) were further modified to delete β_2m by CRISPR-Cas9 (termed here Bw58.MAIT cells). Various APCs (1×10^5) were sorted and cocultured with Bw58.MAIT cells (0.25×10^5) overnight (16 hours) in the presence or absence of titrating amounts of 5-OP-RU at 37°C. MAIT activation was measured by detecting cell surface CD137.

The generation of bone marrow chimeras

Recipient mice were irradiated with 2 × 550 Rads with a 3-hour interval. Irradiated mice were reconstituted with 5×10^6 bone marrow cells (in 200 µl PBS) from the indicated donors. On the next day, mice were injected intraperitoneally with 100 µl anti-Thy1 hybridoma supernatant (clone T24) to deplete recipient T cells that would destroy infected bone marrow cells. Mice were rested for 8 weeks following bone marrow reconstitution.

Bacterial strains and infections

F. tularensis LVS, *L. longbeachae* NSW150 and *S.* Typhimurium BRD509 were cultured as previously reported (*13*–*15*). *F. tularensis* LVS was delivered by means of intravenous injection via the tail vein [10^4 colony-forming units (CFU) in 200 µl PBS], *L. longbeachae* NSW150 and *S.* Typhimurium BRD509 were delivered by means of intranasal administration (10^4 CFU of NSW150 in 50 µl PBS or 5×10^5 CFU of BRD509 in 50 µl PBS). Bacterial colonization was determined by counting the colony forming units (CFU) obtained from plating homogenized organs (lung, liver, and spleen) or lysed peritoneal cavity cells (in 100 µl sterile MilliQ water) from infected mice on CHA agar containing 10 µg/ml ampicillin, 7.5 µg/ml colistin, and 4 µg/ml trimethoprim at 6dpi. Colonies counted after 5 days at 37°C under aerobic conditions.

RNA-seq analysis

Sequencing reads were aligned to the GRCm39 reference genome and transcriptome (version 105) using the STAR aligner (version 2.7.8a) (*66*) and transcript counts established using featureCounts from the subread package (version 2.0.0) (*67*). The data was then analyzed using R (version 4.2.0), limma (version 4.54.1) (*68*) and plots generated with ggplot2 (Wickham, 2016, https://ggplot2.tidyverse.org). To obtain normalised log-expression values, we first filtered the data for lowly or non-expressed genes (filterByExpr function) and normalised counts by TMM (calculateNormFactors), and calculated log-CPM values (cpm).

Human scRNA-seq data

Expression data for *MR1* from the pre-processed and annotated data from lung or blood cells was obtained from published datasets (*36*, *37*). The proportion of cells having a positive expression of *MR1* or *HLA-A* were obtained. A cell with a raw expression value of greater than 0 for each gene was counted as positive.

ATAC-seq

ATAC-seq was performed using the OMNI-ATAC method (*43*). For each cell type, 50,000 cells were sorted and processed. Fragments were barcoded, amplified as described (*43*), and then sequenced using Novaseq X (Illumina). ATAC-Seq raw reads were aligned to the *Mus musculus* GRCm39 reference genome using bwa-mem2 (version 2.2.1) (*69*) and sorted using SAMTools (version 1.16.1) (*70*). ATAC-Seq reads covering the genomic region of *Mr1* were extracted from aligned, sorted .bam files using SAMTools. The remaining analysis and data visualization were performed in R (version 4.2), using tidyverse functions (*71*) and ggpubr (version 0.6.0; Kassambara, 2023, https://rpkgs.datanovia.com/ggpubr). Coverage per genomic position across the length of *Mr1* was calculated by counting the number of reads which included each position. These coverage counts were then normalised to the total library size for each sample, excluding reads mapped to mitochondrial genes. Normalised reads were summed across cell identities ("LPM_SPF," "LPM_GF," "AM_SPF," and "B_SPF") and binned to 100 bases for plotting. To calculate differential accessibility, normalised coverage counts within each peak region were extracted for each sample, the sum of coverage counts under the peak calculated, and averaged over technical replicates. These data were log-transformed to reduce skew and a one-way analysis of variance (ANOVA) was performed for each peak region, followed by a Tukey's test for multiple comparisons.

Microbiome analysis

For microbiome profiling, two 6-week-old female $Mr1^{f/f}$ and $Lyz2^{Cre/+}$-$Mr1^{f/f}$ littermates were cohoused with two 6-week-old female $Mr1^{KO}$ mice for

two weeks. After cohousing, faecal samples and tissues were collected under sterile conditions and placed directly in DNA/RNA Shield (Zymogen). Genomic DNA was extracted and 16S rRNA gene amplicon library construction was performed following the Earth Microbiome Project protocols (https://dx.doi.org/10.17504/protocols.io.kqdg3dzzl25z/v2) and sequenced on an Illumina MiSeq. Sequence data processing and microbiome profiling was performed using the QIIME2 platform (v.2021.4.0) (*72*). Specifically, quality filtering was performed using default cutoffs, Deblur (*73*) was used for sub-operational OTU (sOTU) picking after trimming reads to 150bp, and taxonomic classification was performed using the sklearn-based classifier (*74*) trained on the Greengenes (*75*) 13_8 16S database. Contaminant OTUs were identified and removed by the decontam package (*76*) in R based on their prevalence in negative extraction and sequencing control samples. All subsequent analyses were performed in R (v.4.2.3) using the ape (*77*), clusterProfiler (*78*), limma (*68*), MixOmics (*49*), phyloseq (*79*), qiime2R (https://github.com/jbisanz/qiime2R), rstatix (https://rpkgs.datanovia.com/rstatix; version 0.7.2), tidyverse (*71*), and vegan (https://CRAN.R-project.org/package=vegan; version 2.43) libraries. sOTUs with a mean relative abundance <0.1% across the entire dataset were removed before further analysis.

For alpha diversity analysis, data from each sample type (faecal, skin and lung) were processed separately by rarefying to match the sample with the lowest sequencing depth before calculating Faith's phylogenetic diversity and Shannon's entropy. Differences in alpha diversity between genotypes were determined by ANOVA. Before subsequent analysis, batch correction of microbiome data from separate experiments was performed using the removeBatchEffect function in the limma library on a per sample type basis. Beta diversity was calculated as Aitchison distance (Euclidean distances of batch-corrected, CLR-transformed OTU counts) and visualized by Nonmetric Multidimensional Scaling. Statistical differences between genotypes were determined by PERMANOVA. Partial Least Squares Discriminant Analysis (PLS-DA) was performed on a per-sample type basis using the mixOmics package for R (*49*), and separation of groups along the X and Y axis was determined by ANOVA testing of those coordinates, with post-hoc testing by pairwise *t* test where appropriate. To investigate differences among tissues of $Mr1^{f/f}$ and $Lyz2^{Cre/+}$-$Mr1^{f/f}$ littermates ANCOM-BC2 analysis was performed (*51*). To account for multiple testing, p-values were adjusted using the Benjamini–Hochberg false discovery rate correction, which controls the expected proportion of false discoveries.

For the predicted functional analysis, we used PICRUSt2 under default settings to infer a profile of putative microbial functions (via metagenome prediction) from the 16S rRNA after decontamination and removal of nonbacterial reads (*52*). Representative sequences were analyzed using PICRUSt2 and classified against the Kyoto Encyclopedia of Genes and Genomes (KEGG) Database according to 97% similarity (*80*). For Bugbase analysis, closed reference OTU picking with vsearch was performed on the Deblur-dereplicated sOTU sequences at 97% identity threshold using the Greengenes 13_8 97% rep set database. We then used MaAsLin2, a multivariate statistical model used to identify associations between microbial taxa or functional features and metadata of interest with adjustment on covariates (*81*). We used MaAsLin2 under default settings with a Benjamini-Hochberg corrected P value threshold of 0.2.

Statistical analysis

Statistical analysis was performed using Prism GraphPad (V10.0.3). Comparisons between two groups were performed using a student's *t* test. Comparisons of more than two groups were made using one-way ANOVA for one parameter, or two-way for multiparameter, followed by a multiple comparison test. The following P values were considered statistically significant: $*P < 0.05$, $**P < 0.01$, $***P < 0.001$, and $****P < 0.0001$.

REFERENCES AND NOTES

1. K. Tsukamoto, J. E. Deakin, J. A. Graves, K. Hashimoto, Exceptionally high conservation of the MHC class I-related gene, MR1, among mammals. *Immunogenetics* **65**, 115–124 (2013). doi: 10.1007/s00251-012-0666-5; pmid: 23229473
2. A. J. Corbett *et al.*, T-cell activation by transitory neo-antigens derived from distinct microbial pathways. *Nature* **509**, 361–365 (2014). doi: 10.1038/nature13160; pmid: 24695216
3. L. Kjer-Nielsen *et al.*, MR1 presents microbial vitamin B metabolites to MAIT cells. *Nature* **491**, 717–723 (2012). doi: 10.1038/nature11605; pmid: 23051753
4. S. Mondot, P. Boudinot, O. Lantz, MAIT, MR1, microbes and riboflavin: A paradigm for the co-evolution of invariant TCRs and restricting MHCI-like molecules? *Immunogenetics* **68**, 537–548 (2016). doi: 10.1007/s00251-016-0927-9; pmid: 27393664
5. H. E. G. McWilliam *et al.*, Endoplasmic reticulum chaperones stabilize ligand-receptive MR1 molecules for efficient presentation of metabolite antigens. *Proc. Natl. Acad. Sci. U.S.A.* **117**, 24974–24985 (2020). doi: 10.1073/pnas.2011260117; pmid: 32958637
6. P. Boudinot *et al.*, Restricting nonclassical MHC genes coevolve with TRAV genes used by innate-like T cells in mammals. *Proc. Natl. Acad. Sci. U.S.A.* **113**, E2983–E2992 (2016). doi: 10.1073/pnas.1600674113; pmid: 27170188
7. I. Kawachi, J. Maldonado, C. Strader, S. Gilfillan, MR1-restricted V alpha 19i mucosal-associated invariant T cells are innate T cells in the gut lamina propria that provide a rapid and diverse cytokine response. *J. Immunol.* **176**, 1618–1627 (2006). doi: 10.4049/jimmunol.176.3.1618; pmid: 16424191
8. L. Le Bourhis *et al.*, MAIT cells detect and efficiently lyse bacterially-infected epithelial cells. *PLOS Pathog.* **9**, e1003681 (2013). doi: 10.1371/journal.ppat.1003681; pmid: 24130485
9. T. Leng *et al.*, TCR and inflammatory signals tune human MAIT cells to exert specific tissue repair and effector functions. *Cell Rep.* **28**, 3077–3091.e5 (2019). doi: 10.1016/j.celrep.2019.08.050; pmid: 31533032
10. M. G. Constantinides *et al.*, MAIT cells are imprinted by the microbiota in early life and promote tissue repair. *Science* **366**, eaax6624 (2019). doi: 10.1126/science.aax6624; pmid: 31649166
11. A. D. Smith *et al.*, Microbiota of MR1 deficient mice confer resistance against Clostridium difficile infection. *PLOS ONE* **14**, e0223025 (2019). doi: 10.1371/journal.pone.0223025; pmid: 31560732
12. P. Georgel, M. Radosavljevic, C. Macquin, S. Bahram, The non-conventional MHC class I MR1 molecule controls infection by Klebsiella pneumoniae in mice. *Mol. Immunol.* **48**, 769–775 (2011). doi: 10.1016/j.molimm.2010.12.002; pmid: 21190736
13. H. Wang *et al.*, MAIT cells protect against pulmonary *Legionella longbeachae* infection. *Nat. Commun.* **9**, 3350 (2018). doi: 10.1038/s41467-018-05202-8; pmid: 30135490
14. Z. Zhao *et al.*, *Francisella tularensis* induces Th1 like MAIT cells conferring protection against systemic and local infection. *Nat. Commun.* **12**, 4355 (2021). doi: 10.1038/s41467-021-24570-2; pmid: 34272362
15. Z. Chen *et al.*, Mucosal-associated invariant T-cell activation and accumulation after in vivo infection depends on microbial riboflavin synthesis and co-stimulatory signals. *Mucosal Immunol.* **10**, 58–68 (2017). doi: 10.1038/mi.2016.39; pmid: 27143301
16. A. I. Meierovics, S. C. Cowley, MAIT cells promote inflammatory monocyte differentiation into dendritic cells during pulmonary intracellular infection. *J. Exp. Med.* **213**, 2793–2809 (2016). doi: 10.1084/jem.20160637; pmid: 27799620
17. A. Meierovics, W.-J. C. Yankelevich, S. C. Cowley, MAIT cells are critical for optimal mucosal immune responses during in vivo pulmonary bacterial infection. *Proc. Natl. Acad. Sci. U.S.A.* **110**, E3119–E3128 (2013). doi: 10.1073/pnas.1302799110; pmid: 23898209
18. W. J. Chua *et al.*, Polyclonal mucosa-associated invariant T cells have unique innate functions in bacterial infection. *Infect. Immun.* **80**, 3256–3267 (2012). doi: 10.1128/IAI.00279-12; pmid: 22778103
19. B. van Wilgenburg *et al.*, MAIT cells are activated during human viral infections. *Nat. Commun.* **7**, 11653 (2016). doi: 10.1038/ncomms11653; pmid: 27337592
20. A. Toubal *et al.*, Mucosal-associated invariant T cells promote inflammation and intestinal dysbiosis leading to metabolic dysfunction during obesity. *Nat. Commun.* **11**, 3755 (2020). doi: 10.1038/s41467-020-17307-0; pmid: 32709874
21. O. Rouxel *et al.*, Cytotoxic and regulatory roles of mucosal-associated invariant T cells in type 1 diabetes. *Nat. Immunol.* **18**, 1321–1331 (2017). doi: 10.1038/ni.3854; pmid: 28991267
22. H. Wang *et al.*, IL-23 costimulates antigen-specific MAIT cell activation and enables vaccination against bacterial infection. *Sci. Immunol.* **4**, eaaw0402 (2019). doi: 10.1126/sciimmunol.aaw0402; pmid: 31732518
23. K. Hashimoto, M. Hirai, Y. Kurosawa, A gene outside the human MHC related to classical HLA class I genes. *Science* **269**, 693–695 (1995). doi: 10.1126/science.7624800; pmid: 7624800
24. H. E. McWilliam *et al.*, The intracellular pathway for the presentation of vitamin B-related antigens by the antigen-presenting molecule MR1. *Nat. Immunol.* **17**, 531–537 (2016). doi: 10.1038/ni.3416; pmid: 27043408
25. H. E. G. McWilliam, J. A. Villadangos, MR1 antigen presentation to MAIT cells and other MR1-restricted T cells. *Nat. Rev. Immunol.* **24**, 178–192 (2024). doi: 10.1038/s41577-023-00934-1; pmid: 37773272
26. E. Treiner *et al.*, Selection of evolutionarily conserved mucosal-associated invariant T cells by MR1. *Nature* **422**, 164–169 (2003). doi: 10.1038/nature01433; pmid: 12634786

27. T. S. P. Heng *et al.*, The Immunological Genome Project: Networks of gene expression in immune cells. *Nat. Immunol.* **9**, 1091–1094 (2008). doi: 10.1038/ni1008-1091; pmid: 18800157
28. W. Awad *et al.*, The molecular basis underpinning the potency and specificity of MAIT cell antigens. *Nat. Immunol.* **21**, 400–411 (2020). doi: 10.1038/s41590-020-0616-6; pmid: 32123373
29. J. Y. W. Mak *et al.*, Potent immunomodulators developed from an unstable bacterial metabolite of vitamin B2 biosynthesis. *Angew. Chem. Int. Ed.* **63**, e202400632 (2024). doi: 10.1002/anie.202400632; pmid: 38679861
30. M. C. Gold *et al.*, Human thymic MR1-restricted MAIT cells are innate pathogen-reactive effectors that adapt following thymic egress. *Mucosal Immunol.* **6**, 35–44 (2013). doi: 10.1038/mi.2012.45; pmid: 22692454
31. A. Roquilly, J. D. Mintern, J. A. Villadangos, Spatiotemporal adaptations of macrophage and dendritic cell development and function. *Annu. Rev. Immunol.* **40**, 525–557 (2022). doi: 10.1146/annurev-immunol-101320-031931; pmid: 35130030
32. S. Yona *et al.*, Fate mapping reveals origins and dynamics of monocytes and tissue macrophages under homeostasis. *Immunity* **38**, 79–91 (2013). doi: 10.1016/j.immuni.2012.12.001; pmid: 23273845
33. Z. Liu *et al.*, Fate mapping via Ms4a3-expression history traces monocyte-derived cells. *Cell* **178**, 1509–1525.e19 (2019). doi: 10.1016/j.cell.2019.08.009; pmid: 31491389
34. C. C. Bain *et al.*, Long-lived self-renewing bone marrow-derived macrophages displace embryo-derived cells to inhabit adult serous cavities. *Nat. Commun.* **7**, ncomms11852 (2016). doi: 10.1038/ncomms11852; pmid: 27292029
35. S. Chakarov *et al.*, Two distinct interstitial macrophage populations coexist across tissues in specific subtissular niches. *Science* **363**, eaau0964 (2019). doi: 10.1126/science.aau0964; pmid: 30872492
36. M. Liao *et al.*, Single-cell landscape of bronchoalveolar immune cells in patients with COVID-19. *Nat. Med.* **26**, 842–844 (2020). doi: 10.1038/s41591-020-0901-9; pmid: 32398875
37. E. Stephenson *et al.*, Single-cell multi-omics analysis of the immune response in COVID-19. *Nat. Med.* **27**, 904–916 (2021). doi: 10.1038/s41591-021-01329-2; pmid: 33879890
38. A. N. Keller *et al.*, Drugs and drug-like molecules can modulate the function of mucosal-associated invariant T cells. *Nat. Immunol.* **18**, 402–411 (2017). doi: 10.1038/ni.3679; pmid: 28166217
39. F. Legoux *et al.*, Microbial metabolites control the thymic development of mucosal-associated invariant T cells. *Science* **366**, 494–499 (2019). doi: 10.1126/science.aaw2719; pmid: 31467190
40. R. Emani *et al.*, Peritoneal cavity is a route for gut-derived microbial signals to promote autoimmunity in non-obese diabetic mice. *Scand. J. Immunol.* **81**, 102–109 (2015). doi: 10.1111/sji.12253; pmid: 25410403
41. D. Zhang *et al.*, The cross-talk between gut microbiota and lungs in common lung diseases. *Front. Microbiol.* **11**, 301 (2020). doi: 10.3389/fmicb.2020.00301; pmid: 32158441
42. A. Obers *et al.*, Retinoic acid and TGF-β orchestrate organ-specific programs of tissue residency. *Immunity* **57**, 2615–2633.e10 (2024). doi: 10.1016/j.immuni.2024.09.015; pmid: 39406245
43. F. C. Grandi, H. Modi, L. Kampman, M. R. Corces, Chromatin accessibility profiling by ATAC-seq. *Nat. Protoc.* **17**, 1518–1552 (2022). doi: 10.1038/s41596-022-00692-9; pmid: 35478247
44. P. Meylan, R. Dreos, G. Ambrosini, R. Groux, P. Bucher, EPD in 2020: Enhanced data visualization and extension to ncRNA promoters. *Nucleic Acids Res.* **48** (D1), D65–D69 (2020). doi: 10.1093/nar/gkz1014; pmid: 31680159
45. B. E. Clausen, C. Burkhardt, W. Reith, R. Renkawitz, I. Förster, Conditional gene targeting in macrophages and granulocytes using LysMcre mice. *Transgenic Res.* **8**, 265–277 (1999). doi: 10.1023/A:1008942828960; pmid: 10621974
46. M. C. Abt *et al.*, Commensal bacteria calibrate the activation threshold of innate antiviral immunity. *Immunity* **37**, 158–170 (2012). doi: 10.1016/j.immuni.2012.04.011; pmid: 22705104
47. Y. El Morr *et al.*, MAIT cells monitor intestinal dysbiosis and contribute to host protection during colitis. *Sci. Immunol.* **9**, eadi8954 (2024). doi: 10.1126/sciimmunol.adi8954; pmid: 38905325
48. A. Varelias *et al.*, Recipient mucosal-associated invariant T cells control GVHD within the colon. *J. Clin. Invest.* **128**, 1919–1936 (2018). doi: 10.1172/JCI91646; pmid: 29629900
49. F. Rohart, B. Gautier, A. Singh, K.-A. Lê Cao, mixOmics: An R package for 'omics feature selection and multiple data integration. *PLOS Comput. Biol.* **13**, e1005752 (2017). doi: 10.1371/journal.pcbi.1005752; pmid: 29099853
50. S. J. Robertson *et al.*, Comparison of co-housing and littermate methods for microbiota standardization in mouse models. *Cell Rep.* **27**, 1910–1919.e2 (2019). doi: 10.1016/j.celrep.2019.04.023; pmid: 31067473
51. H. Lin, S. D. Peddada, Multigroup analysis of compositions of microbiomes with covariate adjustments and repeated measures. *Nat. Methods* **21**, 83–91 (2024). doi: 10.1038/s41592-023-02092-7; pmid: 38158428
52. G. M. Douglas *et al.*, PICRUSt2 for prediction of metagenome functions. *Nat. Biotechnol.* **38**, 685–688 (2020). doi: 10.1038/s41587-020-0548-6; pmid: 32483366
53. A. Takeuchi, Electron microscope studies of experimental Salmonella infection. I. Penetration into the intestinal epithelium by *Salmonella typhimurium*. *Am. J. Pathol.* **50**, 109–136 (1967). pmid: 5334433
54. R. Reantragoon *et al.*, Antigen-loaded MR1 tetramers define T cell receptor heterogeneity in mucosal-associated invariant T cells. *J. Exp. Med.* **210**, 2305–2320 (2013). doi: 10.1084/jem.20130958; pmid: 24101382
55. M. Lepore *et al.*, Functionally diverse human T cells recognize non-microbial antigens presented by MR1. *eLife* **6**, e24476 (2017). doi: 10.7554/eLife.24476; pmid: 28518056
56. B. Ruf *et al.*, Tumor-associated macrophages trigger MAIT cell dysfunction at the HCC invasive margin. *Cell* **186**, 3686–3705.e32 (2023). doi: 10.1016/j.cell.2023.07.026; pmid: 37595566
57. Y. Zheng *et al.*, Role of MAIT cells in gastrointestinal tract bacterial infections in humans: More than a gut feeling. *Mucosal Immunol.* **16**, 740–752 (2023). doi: 10.1016/j.mucimm.2023.06.005; pmid: 37353006
58. A. Toubal, I. Nel, S. Lotersztajn, A. Lehuen, Mucosal-associated invariant T cells and disease. *Nat. Rev. Immunol.* **19**, 643–657 (2019). doi: 10.1038/s41577-019-0191-y; pmid: 31308521
59. N. Seach *et al.*, Double-positive thymocytes select mucosal-associated invariant T cells. *J. Immunol.* **191**, 6002–6009 (2013). doi: 10.4049/jimmunol.1301212; pmid: 24244014
60. E. Montassier *et al.*, Robust airway microbiome signatures in acute respiratory failure and hospital-acquired pneumonia. *Nat. Med.* **29**, 2793–2804 (2023). doi: 10.1038/s41591-023-02617-9; pmid: 37957375
61. V. J. Sharma *et al.*, Australian Donation and Transplantation Biobank: A research biobank integrated within a deceased organ and tissue donation program. *Transplant. Direct* **9**, e1422 (2022). doi: 10.1097/TXD.0000000000001422; pmid: 36591329
62. A. J. Kueh *et al.*, An update on using CRISPR/Cas9 in the one-cell stage mouse embryo for generating complex mutant alleles. *Cell Death Differ.* **24**, 1821–1822 (2017). doi: 10.1038/cdd.2017.122; pmid: 28753205
63. J. Y. Mak *et al.*, Stabilizing short-lived Schiff base derivatives of 5-aminouracils that activate mucosal-associated invariant T cells. *Nat. Commun.* **8**, 14599 (2017). doi: 10.1038/ncomms14599; pmid: 28272391
64. W. J. Chua *et al.*, Endogenous MHC-related protein 1 is transiently expressed on the plasma membrane in a conformation that activates mucosal-associated invariant T cells. *J. Immunol.* **186**, 4744–4750 (2011). doi: 10.4049/jimmunol.1003254; pmid: 21402896
65. Z. Chen *et al.*, Characterization and purification of mouse mucosal-associated invariant T (MAIT) cells. *Curr. Protoc. Immunol.* **127**, e89 (2019). doi: 10.1002/cpim.89; pmid: 31763782
66. A. Dobin *et al.*, STAR: Ultrafast universal RNA-seq aligner. *Bioinformatics* **29**, 15–21 (2013). doi: 10.1093/bioinformatics/bts635; pmid: 23104886
67. Y. Liao, G. K. Smyth, W. Shi, The Subread aligner: Fast, accurate and scalable read mapping by seed-and-vote. *Nucleic Acids Res.* **41**, e108 (2013). doi: 10.1093/nar/gkt214; pmid: 23558742
68. M. E. Ritchie *et al.*, limma powers differential expression analyses for RNA-sequencing and microarray studies. *Nucleic Acids Res.* **43**, e47–e47 (2015). doi: 10.1093/nar/gkv007; pmid: 25605792
69. M. Vasimuddin, S. Misra, H. Li, S. Aluru, Efficient architecture-aware acceleration of BWA-MEM for multicore systems. arXiv:1907.12931 [cs.DC] (2019).
70. P. Danecek *et al.*, Twelve years of SAMtools and BCFtools. *Gigascience* **10**, giab008 (2021). doi: 10.1093/gigascience/giab008; pmid: 33590861
71. H. Wickham *et al.*, Welcome to the Tidyverse. *J. Open Source Softw.* **4**, 1686 (2019). doi: 10.21105/joss.01686
72. E. Bolyen *et al.*, Reproducible, interactive, scalable and extensible microbiome data science using QIIME 2. *Nat. Biotechnol.* **37**, 852–857 (2019). doi: 10.1038/s41587-019-0209-9; pmid: 31341288
73. A. Amir *et al.*, Deblur rapidly resolves single-nucleotide community sequence patterns. *mSystems* **2**, e00191-16 (2017). doi: 10.1128/mSystems.00191-16; pmid: 28289731
74. N. A. Bokulich *et al.*, Optimizing taxonomic classification of marker-gene amplicon sequences with QIIME 2's q2-feature-classifier plugin. *Microbiome* **6**, 90 (2018). doi: 10.1186/s40168-018-0470-z; pmid: 29773078
75. T. Z. DeSantis *et al.*, Greengenes, a chimera-checked 16S rRNA gene database and workbench compatible with ARB. *Appl. Environ. Microbiol.* **72**, 5069–5072 (2006). doi: 10.1128/AEM.03006-05; pmid: 16820507
76. N. M. Davis, D. M. Proctor, S. P. Holmes, D. A. Relman, B. J. Callahan, Simple statistical identification and removal of contaminant sequences in marker-gene and metagenomics data. *Microbiome* **6**, 226 (2018). doi: 10.1186/s40168-018-0605-2; pmid: 30558668
77. E. Paradis, K. Schliep, ape 5.0: An environment for modern phylogenetics and evolutionary analyses in R. *Bioinformatics* **35**, 526–528 (2019). doi: 10.1093/bioinformatics/bty633; pmid: 30016406
78. G. Yu, L.-G. Wang, Y. Han, Q.-Y. He, clusterProfiler: An R package for comparing biological themes among gene clusters. *OMICS* **16**, 284–287 (2012). doi: 10.1089/omi.2011.0118; pmid: 22455463
79. P. J. McMurdie, S. Holmes, phyloseq: An R package for reproducible interactive analysis and graphics of microbiome census data. *PLOS ONE* **8**, e61217 (2013). doi: 10.1371/journal.pone.0061217; pmid: 23630581
80. M. Kanehisa, Y. Sato, M. Kawashima, M. Furumichi, M. Tanabe, KEGG as a reference resource for gene and protein annotation. *Nucleic Acids Res.* **44** (D1), D457–D462 (2016). doi: 10.1093/nar/gkv1070; pmid: 26476454

81. H. Mallick *et al.*, Multivariable association discovery in population-scale meta-omics studies. *PLOS Comput. Biol.* **17**, e1009442 (2021). doi: 10.1371/journal.pcbi.1009442; pmid: 34784344

ACKNOWLEDGMENTS

The biospecimens used in this project were provided by the Australian Donation and Transplantation Biobank (ADTB). We acknowledge the contribution of the Victorian Liver Transplant Unit, DonateLife Victoria, and the ADTB to this research project. We gratefully acknowledge the generosity of the deceased organ donors and their families in providing valuable tissue samples. The *Mr1*$^{f/f}$ mouse line was provided by Y. Belkaid and M. Constantinides. We acknowledge the technical assistance of the Translational Research Institute (TRI) Gnotobiotic Facility for the breeding and supply of germfree animals for this study. We thank J. Pooley and C. Yong-Yu Chen for their laboratory management and technical assistance. **Funding:** H.E.G.M. discloses support for the research of this work from the National Health and Medical Research Council of Australia (NHMRC; 2003192) and the CASS Foundation (Medicine/Science Grant). J.A.V. discloses support for the research of this work from the Australian Research Council (ARC; DP170102471), the NHMRC (1113293, 1058193 and 2016969). J.A.V. and D.P.F. acknowledge support from the National Institute of Allergy and Infectious Diseases of the National Institutes of Health (R01AI148407-01A1). A.R. discloses support for the research of this work from Agence National de la Recherche (ANR) (grant ANR JCJC Progr-AM), MSD Avenir (grant PHENOMENON), and European Union's Horizon 2020 research and innovation program under grant agreements 847782 (HAP2) and 101137148 (Homi-lung). H.-F.K. discloses support from the ARC (DE220100830). A.J.C. discloses support from the NHMRC (1193745) and a Dame Kate Campbell Fellowship (University of Melbourne). S.N.M. and Y.O.A. acknowledge funding from the ARC (DP230102108). T.G.P. acknowledges funding from the NHMRC (1139865 and 2026122). T.P. is funded by a Walter Benjamin Postdoctoral Fellowship. J.S. is funded by the J. and M. Wright Foundation. A.H. discloses support from the NHMRC (2018880). D.P.F. acknowledges support from the NHMRC (2009551) and the ARC (CE200100012). L.C. discloses support from the NHMRC (2009339). **Author contributions:** Conceptualization: H.E.G.M., J.A.V., J.D., Y.Y., A.R. Formal analysis: H.E.G.M., J.A.V., J.D., Y.Y., X.Z., C.J.W., E.M., D.S., H.-F.K., N.P., L.D., J.S., A.R. Methodology: H.E.G.M., J.D., Y.Y., A.V., V.J.J., A.P.-G., L.C., A.H., A.J.C., Resources; J.Y.W.M., D.P.F., T.P., L.K.M., Y.O.A., S.N.M., T.P.S., J.K., T.G.P., L.C., A.J.C., A.R. Investigation: H.E.G.M., J.A.V., J.D., Y.Y., X.Z., C.J.W., H.W., A.M., M.A., H.-F.K., T.P., Y.O.A., V.J.J., A.P.-G., Z.C., A.H. Funding acquisition: H.E.G.M., J.A.V., T.G.P., L.C., A.J.C., A.R.. Writing – original draft: H.E.G.M., J.A.V. Writing – review & editing: H.E.G.M., J.A.V., J.D., Y.Y., L.C., A.R., A.J.C., A.H. **Competing interests:** A.R. holds a patent on respiratory microbiome signatures (WO2025078559A2). A.J.C. and J.Y.W.M. are named inventors on a granted patent on the use of 5-OP-RU as an immunological reagent (WO2015/149130, World Intellectual Property Organization) jointly owned by University of Queensland, Monash University, and University of Melbourne. A.J.C. is also an inventor on a patent describing MR1 tetramers (WO/2014/005194), with MR1 tetramers licensed for commercial use to Immudex and for nonprofit use to the NIH Tetramer Core Facility. The other authors declare that they have no competing interests. **Data, code, and materials availability:** The RNA-seq and ATAC-seq datasets are deposited to the NCBI Gene Expression Omnibus and are available under accession nos. GSE306827 and GSE306826, respectively. The microbiome dataset is deposited to the NCBI Sequence Read Archive under accession no. PRJNA1310758. All other data needed to evaluate the conclusions of this study are present in the paper or the supplementary materials. The *Mr1*-tdTomato reporter mice are available from J. Villadangos under a materials transfer agreement with The University of Melbourne.

This research was funded in whole or in part by NHMRC (2003192, 1113293, 1058193, 2016969, 1193745, 1139865, 2026122, 2018880, 2009551, and 2009339) and ANR (ANR JCJC Progr-AM), cOAlition S organizations. The author will make the Author Accepted Manuscript (AAM) version available under a CC BY public copyright license.

SUPPLEMENTARY MATERIALS

science.org/doi/10.1126/science.adr6322
Figs. S1 to S10; MDAR Reproducibility Checklist

Submitted 10 July 2024; resubmitted 16 June 2025; accepted 29 September 2025; published online 4 December 2025

10.1126/science.adr6322

Macrophage MR1 antigen presentation promotes MAIT cell immunity and lung microbiota modulation

Jieru Deng, Yuting Yan, Xiaoyue Zhang, Calum J. Walsh, Emmanuel Montassier, Debajyoti Sinha, Huimeng Wang, Atieh Mousavizadeh, Mitra Ashayeripanah, Jeffrey Y. W. Mak, Hui-Fern Koay, Tobias Poch, Yannick O. Alexandre, Scott N. Mueller, Ajithkumar Vasanthakumar, Tim P. Stinear, Vanta J. Jameson, Alexis Perez-Gonzalez, Jenny Kingham, Tri Giang Phan, Nikita Potemkin, Lachlan Dryburgh, Jan Schroeder, David P. Fairlie, Laura K. Mackay, Zhenjun Chen, Laura Cook, Abderrahman Hachani, Alexandra J. Corbett, Antoine Roquilly, Jose A. Villadangos, and Hamish E. G. McWilliam

Science **391** (6782), eadr6322. DOI: 10.1126/science.adr6322

Editor's summary

Mucosal associated invariant T cells, or MAIT cells, contribute to immune protection against microbial pathogens. These cells are stimulated by other cells that present microbial metabolites using a protein called MHC class I-related protein 1 (MR1), but the identity of these antigen-presenting cells has not been established. Deng *et al*. created a mouse model to facilitate the identification of MR1-expressing cells. Macrophages from the lung and peritoneal cavity expressed the highest levels of MR1 and were efficient at capturing and presenting antigens to MAIT cells. Depletion of MR1 in macrophages impaired the ability of mice to clear systemic and lung bacterial infections and altered the lung microbiota. —Sarah H. Ross